Journal of Theoretical Biology 481 (2019) 28–43

Contents lists available at ScienceDirect

Journal of Theoretical Biology

journal homepage: www.elsevier.com/locate/jtb

Characteristic, completion or matching timescales? An analysis of temporary boundaries in enzyme kinetics

Justin Eilertsen[a], Wylie Stroberg[a], Santiago Schnell[a,b,*]

[a] Department of Molecular & Integrative Physiology, University of Michigan Medical School, Ann Arbor, MI 48109, USA
[b] Department of Computational Medicine & Bioinformatics, University of Michigan Medical School, Ann Arbor, MI 48109, USA

ARTICLE INFO

Article history:
Received 8 September 2018
Revised 31 December 2018
Accepted 4 January 2019
Available online 5 January 2019

Keywords:
Timescales
Chemical kinetics
Enzyme kinetics
Slow and fast dynamics
Perturbation methods
Nonlinear dynamical systems

ABSTRACT

Scaling analysis exploiting timescale separation has been one of the most important techniques in the quantitative analysis of nonlinear dynamical systems in mathematical and theoretical biology. In the case of enzyme catalyzed reactions, it is often overlooked that the characteristic timescales used for the scaling the rate equations are not ideal for determining when concentrations and reaction rates reach their maximum values. In this work, we first illustrate this point by considering the classic example of the single-enzyme, single-substrate Michaelis–Menten reaction mechanism. We then extend this analysis to a more complicated reaction mechanism, the auxiliary enzyme reaction, in which a substrate is converted to product in two sequential enzyme-catalyzed reactions. In this case, depending on the ordering of the relevant timescales, several dynamic regimes can emerge. In addition to the characteristic timescales for these regimes, we derive matching timescales that determine (approximately) when the transitions from transient to quasi-steady-state kinetics occurs. The approach presented here is applicable to a wide range of singular perturbation problems in nonlinear dynamical systems.

1. Introduction

Nonlinear differential equations are used to model the dynamical behavior of natural phenomena in science. As the natural phenomena become more complex, the dynamics are influenced by multiple timescales, which create technical problems in the mathematical analysis and numerical computation of models (Lin and Segel, 1988).

The 21st century has been dominated by advances in the biological and biomedical sciences. As a result, examples of complex dynamical systems have become ubiquitous in theoretical and mathematical biology. Despite their complexity, all major levels of biological organization have one common dynamical denominator: chemical reactions are continuously taking place in living systems. Most of these reactions involve enzymes. Arguably, if biology is to be understood as a dynamical process, enzyme catalyzed reactions need to be investigated quantitatively (Gallagher, 2004).

The quantitative description of any enzyme catalyzed chemical reaction is often decomposed into two categories: thermodynamics and kinetics. The former tells us if a particular reaction is favorable, while latter describes the timescales over which reactions occur. From the point of view of the experimental scientist, chemical kinetics focuses on the measurement of concentrations as a function of time with the goal of characterizing reaction properties (Espenson, 1995). Regardless of whether a kinetic model is linear or nonlinear, stochastic or deterministic, the effectiveness of the model is only as good as the timescales it predicts (Shoffner and Schnell, 2017): timescales provide not only an estimation of the effective duration of the reaction, but are also critical in characterizing reaction mechanisms. This topic is not unfamiliar to Philip K. Maini, who has worked in a number of diverse areas of mathematical biology, including enzyme kinetics (Burke et al., 1993, 1990; Frenzen and Maini, 1988; Schnell and Maini, 2000, 2002, 2003).

Philip K. Maini mentored one of us, Santiago Schnell, through the rigorous theory of timescale analysis in chemical kinetics that lies at the intersection of chemistry and geometric singular perturbation theory (GSPT). In fact, GSPT is widely applicable not only to chemical kinetics, but to a plethora of important biological models (Bertram and Rubin, 2017). Largely, GSPT is the study of dynamical systems of the form

$$\dot{x} = f(x, y), \tag{1a}$$

$$\varepsilon \dot{y} = g(x, y), \tag{1b}$$

where $\varepsilon \ll 1$, and "$\cdot$" denotes differentiation with respect to time. These systems are often referred to as slow/fast systems, since

* Corresponding author at: Molecular & Integrative Physiology, 1137 E. Catherine St., Ann Arbor, MI 48109-5622, United States.
E-mail address: schnells@umich.edu (S. Schnell).

https://doi.org/10.1016/j.jtbi.2019.01.005
0022-5193/

changes in the variable x occur over timescales that are large compared to the timescales over which the variable y changes. For example, if time is rescaled as $t_\varepsilon = t/\varepsilon$, then the evolution of (1) becomes

$$x' = \varepsilon f(x, y), \tag{2a}$$

$$y' = g(x, y), \tag{2b}$$

with $'$ denoting differentiation with respect to t_ε. Over the t_ε-timescale, the variable x barely changes, while the variable y can change significantly. In contrast, the change in variable x is non-trivial over the t-timescale and, due to the presence of slow manifolds (Roussel and Fraser, 1990), the change in the variable y can be shown to be explicitly dependent on change in x. Thus, the dynamics of (1) is dependent on two different timescales: the fast timescale, t_ε, and the slow timescale, t. Each timescale defines a unique dynamical regime: the initial, "t_ε-regime", over which x is essentially constant and y changes rapidly, and the "t-regime", in which x changes significantly and the change in y is dependent on the change in x.

GSPT has a rich relationship with chemical kinetics, particularly regarding the application of *matched asymptotics*. Matched asymptotics is a common mathematical approach aimed at finding an accurate approximation to the solution of an equation, or system of equations (see Kuehn, 2015, for an excellent discussion on matched asymptotics). Usually, the study of matched asymptotics is linked to singular perturbation problems that arise as a consequence of underlying disparate spatial layers, such as boundary layers that form in pattern formation during embryonic development (see Maini et al., 2012). The specific aim of matched asymptotics is to generate a *composite solution*, which is constructed by gluing together local solutions (solutions that are asymptotically valid on different regimes) to comprise a solution that is uniformly valid (Holmes, 2013). Of principal interest in chemical kinetics, for which there typically exist multiple disparate timescales, is to determine the timescales that contribute to the composite solution.

In this work, we begin by introducing the characteristic timescale, which is a well-defined timescale from dynamical systems theory. We show that the established "fast timescale" of the single-enzyme, single-substrate, Michaelis–Menten (MM) reaction mechanism is in fact a characteristic timescale, and we demonstrate that characteristic timescales do provide a correct "partitioning" of time into the different slow and fast sub-domains from which the composite solution should be constructed. However, we also show that characteristic timescales are not suitable for determining *when* a transition from one dynamical regime to another dynamical regime occurs. This means that characteristic timescales cannot tell us when concentrations of certain chemical species reach their peak values, or when the rate of product generation reaches its maximum value. Thus, there is a need for an additional timescale, which we refer to as a *matching timescale*, that provides a temporal boundary between specific dynamic (kinetic) regimes. Its derivation follows directly from the theory of GSPT and matched asymptotics, and we demonstrate that appropriate matching timescales can be constructed from physical knowledge of the characteristic timescales. Specifically, through the application of Tikhonov–Fenichel Theory (Fenichel, 1971; Tikhonov, 1952), we derive the correct matching timescale for the MM reaction mechanism, and show that it can be explicitly obtained from the fast and slow characteristic timescales. We also categorize the corresponding slow timescale of the MM reaction mechanism as either a characteristic, depletion, or completion timescale.

Most chemical reactions that consist of two disparate timescales are well-understood. However, much of the modern GSPT analyzes problems comprising *more* than two timescales (Letson et al., 2017; Nan et al., 2015; Vo et al., 2013), and it is time to push enzyme kinetics in this direction. Thus, in this work, we analyze the kinetics of the auxiliary enzyme reaction mechanism (Eilertsen and Schnell, 2018)

$$S_1 + E_1 \underset{k_{-1}}{\overset{k_1}{\rightleftharpoons}} C_1 \overset{k_2}{\rightarrow} E_1 + S_2,$$

$$S_2 + E_2 \underset{k_{-3}}{\overset{k_3}{\rightleftharpoons}} C_2 \overset{k_4}{\rightarrow} E_2 + P,$$

under the assumption that the auxiliary enzyme, E_2, is in excess with respect to E_1. We show that there are four timescales in a certain parameter regime of this reaction, and we illustrate that different orderings of the timescales must be considered in order to establish a complete description of the kinetics. The relevant characteristic timescales that approximate the duration of each regime are derived through geometric analysis of the phase-plane. Lastly, composite solutions and matching timescales are obtained.

2. The characteristic timescale

Consider a general, autonomous dynamical system of the form

$$\dot{x} = f(x), \tag{3}$$

and suppose $f(x)$ has a fixed point, x^*, such that $f(x^*) = 0$. The *characteristic timescale* is the reciprocal of the exponential growth/decay constant of the linearized equation in a small neighborhood surrounding x^*. That is, if δ is a small perturbation, then

$$f(x^* + \delta) \simeq \delta \frac{df}{dx}|_{x=x^*} \equiv \delta f'(x^*), \tag{4}$$

and therefore

$$\dot{\delta} \simeq f'(x^*)\delta. \tag{5}$$

Since linearized evolution of the perturbation grows or decays according to

$$\delta = \delta(0) \exp\left[f'(x^*)t\right], \tag{6}$$

the characteristic timescale, t_χ, is the time required for the perturbation to *significantly* grow or decay:

$$t_\chi = \frac{1}{|f'(x^*)|}. \tag{7}$$

For a linear, exponential decay differential equation of the form

$$\dot{x} = -\gamma x, \quad x(0) = x_0, \tag{8}$$

the characteristic timescale is $1/\gamma$, and corresponds to the exact amount of time it takes the initial condition to decay to

$$x(t_\chi) = (1 - \ell)x_0, \quad \ell = \frac{\exp(1) - 1}{\exp(1)}, \tag{9}$$

which is roughly $0.37x_0$. In addition, for a linear equation of the form

$$\dot{x} = -\gamma x + A, \quad x(0) = 0, \tag{10}$$

where A is a constant, the characteristic timescale, $1/\gamma$, is the exact amount of time it takes x to grow to

$$x(t_\chi) = \ell \frac{A}{\gamma} \equiv \ell x^{\max}, \tag{11}$$

or roughly $0.63x^{\max}$.

3. The slow and fast timescales of the Michaelis–Menten reaction mechanism: An exercise in the power and limitations of characteristic timescales

We continue by reviewing the pertinent characteristic timescales for the well-studied single-enzyme, single-substrate reaction mechanism (12), in which an enzyme, E_1, binds to a substrate, S_1 (forming an intermediate enzyme-substrate complex, C_1), and catalyzes the conversion of S_1 into product, P:

$$S_1 + E_1 \underset{k_{-1}}{\overset{k_1}{\rightleftharpoons}} C_1 \overset{k_2}{\rightarrow} E_1 + P. \tag{12}$$

The kinetics of the reaction depend not only in the rate constants, k_1 and k_{-1}, and the catalytic constant k_2, but also on the initial concentrations of S_1 and E_1. Specifically, the *reduced* mass action equations that govern the kinetics of (12) are

$$\dot{s}_1 = -k_1(e_1^0 - c_1)s_1 + k_{-1}c_1, \tag{13a}$$

$$\dot{c}_1 = k_1(e_1^0 - c_1)s_1 - (k_{-1} + k_2)c_1. \tag{13b}$$

In this system, s_1 denotes the concentration of S_1, c_1 denotes the concentration of C_1, and s_1^0 and e_1^0 are, respectively, the initial substrate and enzyme concentrations. The mass action Eqs. (13a)–(13b) can be approximated with the differential-algebraic equation,

$$\dot{s}_1 = -\frac{e_1^0 k_2 k_1}{k_{-1} + k_2 + k_1 s_1} s_1, \tag{14a}$$

$$c_1 = \frac{k_1 e_1^0}{k_{-1} + k_2 + k_1 s_1} s_1, \tag{14b}$$

by assuming the quasi-steady-state approximation (QSSA).

Despite a significant body of literature dedicated to the development of methods and techniques for estimating timescales in chemical kinetics (Palsson, 1987; Palsson and Lightfoot, 1984; Palsson et al., 1985; Rice, 1960; Segel, 1988; Segel and Slemrod, 1989; Shoffner and Schnell, 2017), timescale estimation remains *ad hoc* in most applications, and we will later see that this work is no exception. We will study and review (12) in regimes where the QSSA is valid. Historically, the most common method employed to study the validity of the QSSA is scaling combined with singular perturbation analysis. Early studies (Heineken et al., 1967) of the validity of the QSSA suggested that the initial enzyme concentration must be small in comparison to the initial substrate concentration: $\bar{\varepsilon} \equiv e_1^0/s_1^0 \ll 1$. One of the first authors to recognize that $\bar{\varepsilon} \ll 1$ was an incomplete condition for the validity of the QSSA was Bernhard Palsson (Palsson, 1987; Palsson and Lightfoot, 1984). Palsson made two important discoveries: (1) he recognized that the QSSA was still applicable when $e_1^0 \approx s_1^0$ as long as $e_1^0 \ll (k_{-1} + k_2)/k_1$; (2) he noted that the QSSA is *still* valid when $e_1^0 \approx s_1^0 \approx (k_{-1} + k_2)/k_1$ as long as $\kappa_1 \equiv k_{-1}/k_2 \gg 1$. About a year later, Segel (1988), who understood that there was subtle difference between non-dimensionalization and scaling, correctly estimated the disparate timescales of complex formation and substrate depletion. In short, the earlier studies failed to determine necessary conditions for the validity of the QSSA because, although time had been properly non-dimensionalized in previous analyses, it had not been appropriately *scaled*. Thus, history tells us that it is difficult, if not impossible, to determine necessary conditions for the validity of reduction techniques (like the QSSA) when slow and fast timescales are unknown. We will review Segel's analysis in the forthcoming subsections. In addition, we will show that the timescales derived by Segel can be used to approximate the matching timescale, which gives a better estimation of the time it takes for the reaction to reach quasi-steady-state (QSS).

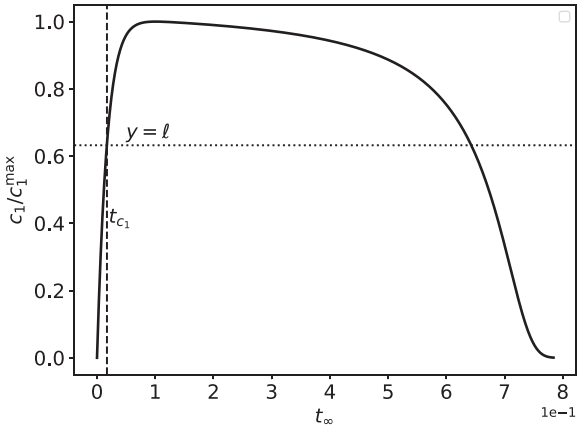

Fig. 1. The validity of t_{c_1} for the Michaelis-Menten reaction mechanism (12). The solid black curve is the numerically-computed solution to (13a)–(13b). The dashed vertical curve is corresponds to $t_{c_1} = [k_1(K_{M_1} + s_1^0)]^{-1}$. The dotted horizontal line corresponds to $\ell c_1/c_1^{\max} = \ell$. The initial concentrations and rate constants used in the numerical simulation are: $k_1 = 0.1$, $k_2 = 10$, $k_{-1} = 1$, $e_1^0 = 1$ and $s_1^0 = 100$ (units have been omitted). Time has been mapped to the t_∞ scale: $t_\infty(t) = 1 - 1/\ln[t + \exp(1)]$.

3.1. The characteristic initial fast transient of the reaction

It is well-established that, under the reactant stationary assumption (RSA, Hanson and Schnell, 2008; Schnell, 2014), the dynamics of (12) initialize with a brief initial transient during which the intermediate complex concentration, c_1, accumulates rapidly towards its maximum while the substrate s_1 remains effectively unchanged from the initial substrate concentration s_1^0. The RSA ensures $s_1 \approx s_1^0$ during the initial transient of the reaction. Under the RSA, Eq. (13b) is approximately

$$\dot{c}_1 \simeq k_1(e_1^0 - c_1)s_1^0 - (k_{-1} + k_2)c_1, \tag{15}$$

which admits the solution

$$c_1 \simeq c_1^{\max}\left[1 - \exp(-k_1(K_{M_1} + s_1^0)t)\right], \quad c_1^{\max} = \frac{e_1^0 s_1^0}{K_{M_1} + s_1^0}. \tag{16}$$

In the above equation, $K_{M_1} = (k_{-1} + k_2)/k_1$ is the Michaelis constant. The characteristic timescale of the intermediate complex that arises from (16) is t_{c_1}:

$$t_{c_1} = \frac{1}{k_1(K_{M_1} + s_1^0)}. \tag{17}$$

Technical justification for t_{c_1} was originally obtained by Segel (1988) and Segel and Slemrod (1989). Through scaling analysis, they introduced the dimensionless parameters

$$\sigma_1 \equiv \frac{s_1^0}{K_{M_1}}, \quad \kappa_1 \equiv k_{-1}/k_2, \quad \beta_1 \equiv \frac{1}{1+\sigma_1} < 1, \quad \alpha_1 \equiv \frac{\kappa_1}{1+\kappa_1} < 1, \tag{18}$$

allowing Eqs. (13a)–(13b) to be rescaled into their dimensionless form

$$\begin{aligned} \frac{d\hat{s}_1}{d\tau} &= \varepsilon_1\left[-\hat{s}_1 + (1-\beta_1)\hat{c}_1\hat{s}_1 + \beta_1\alpha_1\hat{c}_1\right], \quad \varepsilon_1 = \frac{e_1^0}{K_{M_1} + s_1^0} \\ \frac{d\hat{c}_1}{d\tau} &= \hat{s}_1 - (1-\beta_1)\hat{c}_1\hat{s}_1 - \beta_1\hat{c}_1, \end{aligned} \tag{19}$$

where $\tau = t/t_{c_1}, \hat{s}_1 = s_1/s_1^0$ and $\hat{c}_1 = c_1/c_1^{\max}$. It is clear from (19) that if $\varepsilon_1 \ll 1$, then $s_1 \simeq s_1^0$ when $t \leq t_{c_1}$. Formally, the qualifier $\varepsilon_1 \ll 1$ *is* the condition for the RSA, and t_{c_1} is the *characteristic* timescale of the initial fast transient (see Fig. 1).

3.2. The slow timescale of the MM reaction: From characteristic to completion

In contrast to the brief timescale over which c_1 accumulates (i.e, t_{c_1}), s_1 changes over a much longer timescale. The timescale over which there is appreciable change in s_1 is the slow timescale of the reaction or the substrate depletion timescale. As a direct result of singular perturbation theory, the depletion of s_1 is approximately

$$\dot{s}_1 \simeq -\frac{V_1}{K_{M_1}+s_1}s_1 \tag{20}$$

after the initial fast transient (i.e. for $t > t_{c_1}$). The above expression, obtained from the QSSA, is known as the MM equation (see, Schnell, 2014; Schnell and Maini, 2003, for reviews), and $V_1 = k_2 e_1^0$ is the limiting rate of the reaction. The slow timescale, t_{s_1}, is given by

$$t_{s_1} = \frac{s_1^0}{\max|\dot{s}_1|} = \frac{K_{M_1}+s_1^0}{V_1}. \tag{21}$$

The technical justification of (21) is acquired through scaling analysis. By writing the dimensionless form (13a)–(13b) with respect to $T = t/t_{s_1}$ yields

$$\begin{aligned}\frac{d\hat{s}_1}{dT} &= (1+\kappa_1)(1+\sigma_1)\left[-\hat{s}_1 + (1-\beta_1)\hat{c}_1\hat{s}_1 + \beta_1\alpha_1\hat{c}_1\right],\\ \varepsilon_2\frac{d\hat{c}_1}{dT} &= \hat{s}_1 - (1-\beta_1)\hat{c}_1\hat{s}_1 - \beta_1\hat{c}_1.\end{aligned} \tag{22}$$

The dimensionless parameter, ε_2, is the ratio of fast and slow timescales: $\varepsilon_2 = t_{c_1}/t_{s_1}$.

While mathematicians typically refer to t_{s_1} as the slow timescale, the chemical interpretation of t_{s_1} depends on the initial *specific concentration*, σ_1. First, the MM Eq. (20) admits a closed-form solution with $s_1(t=0) = s_1^0$

$$s_1 = K_{M_1} W[\sigma_1 \exp(\sigma_1 - \eta_1 t)], \quad \eta_1 = \frac{V_1}{K_{M_1}}, \tag{23}$$

where $W[\cdot]$ is the Lambert-W function (Corless et al., 1996; Schnell and Mendoza, 1997), and the closed-form solution is known as the Schnell–Mendoza equation (Clark et al., 2011; Feng et al., 2014; Murugan, 2018; Son et al., 2015). If $\sigma_1 \ll 1$, then (23) is asymptotic to

$$s_1 \simeq s_1^0 \exp(-\eta_1 t), \tag{24}$$

from which we obtain:

$$s_1(t_{s_1}) \simeq (1-\ell)s_1^0. \tag{25}$$

Thus, if the initial substrate concentration is much less than the Michaelis constant, K_{M_1}, then the slow timescale, t_{s_1}, *is* a characteristic timescale for the substrate species (see Fig. 2).

The calculus of the Lambert-W function determines the relevant chemical interpretation of t_{s_1} as σ_1 increases. When $t = t_{s_1}$, the substrate concentration is, based on the RSA, $K_{M_1}W[(1-\ell)\sigma_1]$. Furthermore,

$$W[u] \ll u, \quad \text{when } 1 \ll u, \tag{26}$$

and we see from (26) that as the argument "u" gets large, the distance from u to $W[u]$ gets greater. Since

$$s_1(t_{s_1}) = K_{M_1}W[(1-\ell)\sigma_1)], \tag{27}$$

it follows from (26) that

$$W[(1-\ell)\sigma_1] \ll (1-\ell)\sigma_1 \tag{28}$$

as σ_1 gets large. Thus, for large σ_1, it holds that

$$s_1(t_{s_1}) \ll (1-\ell)s_1^0, \tag{29}$$

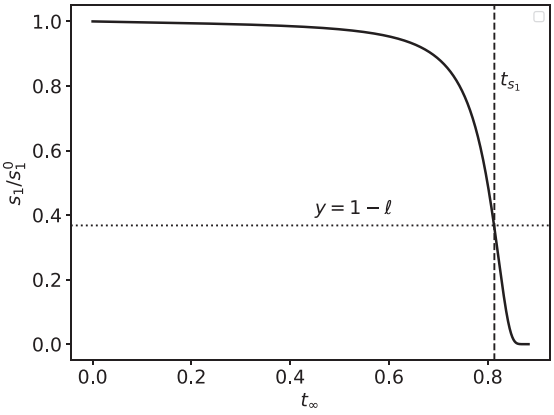

Fig. 2. The graphical illustration of the characteristic timescale for the Michaelis–Menten reaction mechanism (12). When $\sigma_1 \ll 1$, the timescale t_{s_1} is the characteristic time of the substrate species. The solid black curve is the numerical solution to the mass action Eqs. (13a)–(13b) and the vertical dashed/dotted line corresponds to $t = t_{s_1}$. The dotted horizontal line corresponds to the scaled characteristic value $(1-\ell)s_1^0$. The constants (without units) used in the numerical simulation are: $e_1^0 = 1, k_1 = 0.01, k_2 = 10, k_{-1} = 1$ and $s_1^0 = 100$. Time has been mapped to the t_∞ scale: $t_\infty(t) = 1 - 1/\ln[t + \exp(1)]$.

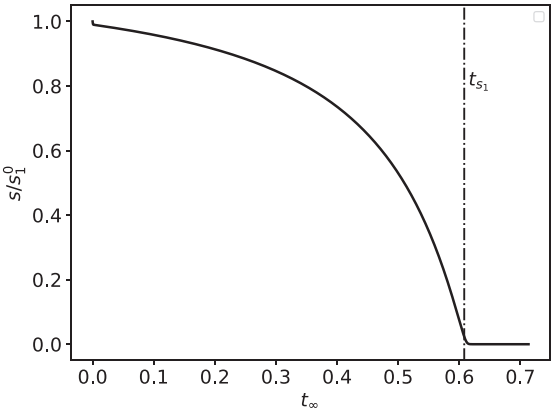

Fig. 3. The graphical illustrations of the completion timescale for the Michaelis–Menten reaction mechanism (12). When $\sigma_1 \gg 1$, the reaction is essentially complete when $t = t_{s_1}$. The solid black curve is the numerical solution to the mass action Eqs. (13a)–Eqs. (13b) and the vertical dashed/dotted line corresponds to $t = t_{s_1}$. The constants (without units) used in the numerical simulation are: $e_1^0 = 1, k_1 = 10, k_2 = 10, k_{-1} = 1$ and $s_1^0 = 100$. Time has been mapped to the t_∞ scale: $t_\infty(t) = 1 - 1/\ln[t + \exp(1)]$.

in which case we categorize t_{s_1} as a *completion timescale*, since it is proportional to the total length of the reaction (see Fig. 3).

In the intermediate range, when neither $\sigma_1 \ll 1$ or $\sigma_1 \gg 1$ holds, t_{s_1} is still the appropriate timescale over which a *significant* reduction in substrate concentration occurs, and in this case we refer to the slow timescale as the *depletion timescale*, since it is too long to be a characteristic timescale, but too short to be a completion timescale.

3.3. The QSSA versus the RSA

How did Segel's work reconcile the work of Heineken et al. (1967) with the observations made by Palsson (1987)? In a nutshell, Segel and Slemrod (1989) found that over the fast timescale the mass action equations scale as

$$\dot{\hat{s}}_1 = \varepsilon_1 f(\hat{s}_1, \hat{c}_1), \tag{30a}$$

$$\dot{\hat{c}}_1 = g(\hat{s}_1, \hat{c}_1), \tag{30b}$$

and on the slow timescale as

$$\hat{s}_1' = \tilde{f}(\hat{s}_1, \hat{c}_1), \tag{31a}$$

$$\varepsilon_2 \hat{c}_1' = \tilde{g}(\hat{s}_1, \hat{c}_1), \tag{31b}$$

where f, g denote the right hand sides of (19), and $\tilde{f}, \tilde{g}$ denotes the right hand sides of (22). If $\varepsilon_1 \ll 1$, then the depletion of substrate over the fast timescale is negligible. However, if $\varepsilon_1 \approx 1$, but $\varepsilon_2 \ll 1$, then the QSSA is still valid after an initial transient. The distinguishing feature in the case when $\varepsilon_2 \ll \varepsilon_1 \sim 1$ is that the depletion of s_1 over the initial transient is noticeable (Segel and Slemrod, 1989).

It is straightforward to the show that $\varepsilon_2 < \varepsilon_1$. Consequently, the condition for the validity of the RSA, $\varepsilon_1 \ll 1$, ensures the validity of the QSSA on the slow timescale. Moreover, since $\varepsilon_1 \ll 1$ guarantees that the depletion of s_1 minimal over t_{c_1}, the qualifier $\varepsilon_1 \ll 1$ ensures the validity of the QSSA for the entire dynamics of the reaction (12) (Hanson and Schnell, 2008).

3.4. Matched asymptotics: The composite solution for the time course of the reaction

Expressing the asymptotic solution to (13a)–(13b) as,

$$\begin{cases} s_1 \simeq s_1^0, \\ c_1 \simeq c_1^{\max}[1 - \exp(-t/t_{c_1})], \end{cases} \qquad t \le t_{c_1} \tag{32a}$$

$$\begin{cases} s_1 \simeq K_{M_1} W[\sigma_1 \exp(\sigma_1 - \eta_1 t)], \\ c_1 \simeq \dfrac{e_1^0}{K_{M_1} + s_1} s_1, \end{cases} \qquad t > t_{c_1} \tag{32b}$$

serves well to convey the fact that the dynamics of the reaction changes depending on where a particular time point falls in relation to t_{c_1}, and these equations provide us with the correct inner and outer solutions that approximate the kinetics under the RSA. However, it is well-understood that Eqs. (32a)–Eqs. (32b) are misleading: there is a large transition regime surrounding t_{c_1} and, within this transition regime, the outer solution (32b) does not accurately approximate the true solution. Note that the presence of a transition regime does not suggest that t_{c_1} is an inappropriate timescale. In fact, the timescales derived in the previous section are *the* appropriate timescales that categorize the fast and slow regimes of the reaction. To see why, and to mitigate the effect of the transition region, we construct the *composite solution* for the intermediate complex, c_1^{io}:

$$c_1^{io} = \frac{e_1^0}{K_{M_1} + s_1} s_1 - c_1^{\max} \exp(-t/t_{c_1}). \tag{33}$$

The composite solution provides a uniform asymptotic solution that is valid for all time. Furthermore, the accuracy of (33) indicates that t_{c_1} and t_{s_1} quantify the appropriate temporal length scales of the initial fast transient and quasi-steady-state regime (see Fig. 4).

3.5. The characteristic timescale is not a matching timescale

From a theoretical point of view, the composite solution has little advantage over the numerical solution in terms of estimating *when* the transition to the quasi-steady-state phase occurs. We will refer to the time at which the transition to QSS occurs as a *matching timescale*, and a rough candidate for a matching timescale is t_{c_1}. The caveat with utilizing t_{c_1} as a matching timescale is that t_{c_1} is a characteristic timescale, and hence will only provide characteristic (as opposed to limiting) values of the concentrations within a given regime. To clearly illustrate why t_{c_1} fails to be an adequate matching timescale requires a phase–plane analysis of the mass action Eqs. (13a)–Eqs. (13b). After the initial buildup of the intermediate, c_1, the phase–plane trajectory is asymptotic to a slow manifold, $\mathcal{M}_\varepsilon$. The slow manifold is invariant, and is at a $\mathcal{O}(\varepsilon_2)$-distance from the c_1-nullcline, $\mathcal{M}_0$:

$$\mathcal{M}_0 = \left\{ (s_1, c_1) : c_1 - \frac{e_1^0}{K_{M_1} + s_1} s_1 = 0 \right\}. \tag{34}$$

The outer solution, (32b), is valid once the trajectory is *extremely close* to the slow manifold, which implies c_1 should be near its maximum value at the onset of outer solution validity. The complex reaches its maximum value once the trajectory reaches $\mathcal{M}_0$. However, when $t = t_{c_1}$, the concentration of the complex is far enough away from its maximum value to render the outer solution invalid:

$$c_1(t_{c_1}) \approx \ell c_1^{\max} < c_1^{\max}. \tag{35}$$

Thus, $c_1(t_{c_1}) \notin \mathcal{M}_0$, and therefore the trajectory is not quite close enough to $\mathcal{M}_\varepsilon$ to justify (32b) as an asymptotic solution (see Fig. 2).

A more accurate estimate of the actual time it takes c_1 to reach its maximum concentration (we will denote this timescale as $t_{c_1}^*$) can be obtained by either: (i) solving the mass action equations exactly or, (ii) by means of an asymptotic approximation. Employing strategy (i) is difficult due to the nonlinearity of the equations; strategy (ii) tends to be more straightforward to implement. If we utilize (ii), we immediately meet an obvious conundrum if we try to estimate $t_{c_1}^*$ directly from (32a) or (32b): (32a) predicts that it will take an infinite amount of time for c_1 to reach $c_1^{\max}$, while (32b) predicts $t_{c_1}^* = 0$. To work around this, we look for an asymptotic estimate to $t_{c_1}^*$. Starting with the inner solution,

$$c_1(\tau) = c_1^{\max}[1 - \exp(-\tau)] \tag{36}$$

we rewrite (36) in terms of the slow timescale, $T = t/t_{s_1}$:

$$c_1(T) = c_1^{\max}[1 - \exp(-T/\varepsilon_2)]. \tag{37}$$

By inspection of (37), we see that c_1 *should* be in an $\mathcal{O}(\varepsilon_2)$-neighborhood of the slow manifold when

$$T = \varepsilon_2 |\ln \varepsilon_2|. \tag{38}$$

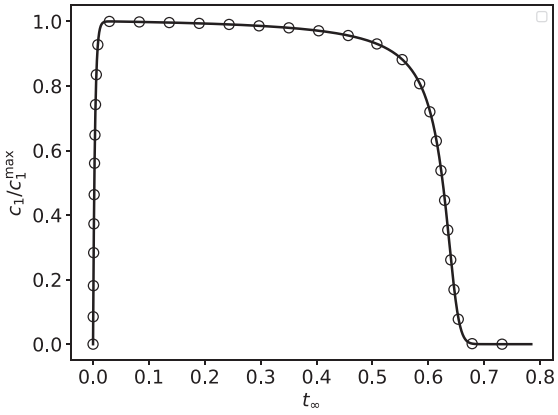

Fig. 4. A graphical comparison of the composite and numerical solutions for the time course of the Michaelis–Menten reaction (12). The solid black curve is the numerical solution to (13a)–(13b). The unfilled circles mark the composite solution (33). The initial concentrations and rate constants used in the numerical simulation are: $k_1 = 1$, $k_2 = 1$, $k_{-1} = 1$, $e_1^0 = 1$ and $s_1^0 = 100$ (units have been omitted). All approximations have been scaled by their numerically–obtained maximum values, and time has been mapped to the t_∞ scale: $t_\infty(t) = 1 - 1/\ln[t + \exp(1)]$.

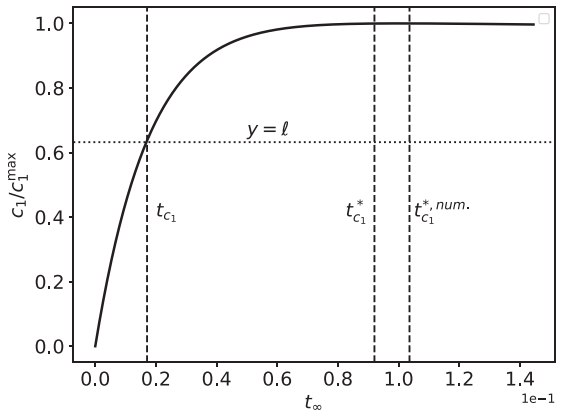

Fig. 5. The validity of $t^*_{c_1}$ and a graphical representation of its comparison with t_{c_1} for the Michaelis–Menten reaction mechanism (12). The solid black curve is the numerically-computed solution to (13a)–(13b). The left-most dashed vertical curve is corresponds to t_{c_1}, and the middle dashed vertical curve corresponds to the estimated value $t^*_{c_1} = -t_{c_1} \ln \varepsilon_2$. The dashed vertical line corresponds to the numerically-computed $t^*_{c_2}$, which is labeled as $t^{*,num}_{c_1}$ in the figure. Notice that $t^*_{c_1}$ provides a much better estimate of the time it takes c_1 to reach its maximum than t_{c_1}. The initial concentrations and rate constants used in the numerical simulation are: $k_1 = 0.1$, $k_2 = 10$, $k_{-1} = 1$, $e^0_1 = 1$ and $s^0_1 = 100$ (units have been omitted). Time has been mapped to the t_∞ scale: $t_\infty(t) = 1 - 1/\ln[t + \exp(1)]$. Note that the mass action equations have only been integrated from $t = 0$ to $t \approx t^*_{c_1}$ for clarity.

Next, since $T = t/t_{s_1}$, we solve for t in (38) to obtain an asymptotic estimate on $t^*_{c_1}$:

$$t^*_{c_1} \simeq -t_{c_1} \ln \varepsilon_2. \tag{39}$$

The timescale (39) is the matching timescale, although various authors refer to any timescale of order $\varepsilon|\ln\varepsilon|$ as simply *a slow time* (Kuehn, 2015). While not exact, the approximation (39) provides a useful estimate of the time to transition from transient to quasi-steady-state kinetics for the single-enzyme, single-substrate MM reaction mechanism (see Fig. 5).

As a final remark, we note that the asymptotic approximation (39) is not without a more rigorous justification. So far, we have been able to estimate matching timescales by directly calculating them from the "inner" or transient solution; the direct method is possible because we have closed-form solutions comprised of exponential functions. However, for a generic fast/slow dynamical system of the form

$$\dot{x} = f(x, y), \tag{40a}$$

$$\varepsilon \dot{y} = g(x, y), \tag{40b}$$

the equation $\dot{y} = g(x_0, y)$ may not be linear, and a closed-form solution may not be available. However, it is a well-known fact, stated in both textbooks (Kuehn, 2015) and literature (Klonowski, 1983), that the time necessary for the fast-variable to reach QSS is generally $\mathcal{O}(\varepsilon|\ln\varepsilon|)$. This result is due to the work of Tikhonov (1952), who studied the convergence of the solution to the perturbed system (40a)–(40b) to the solution of the degenerate system, (41a)–(41b):

$$\dot{x} = f(x, y), \tag{41a}$$

$$0 = g(x, y). \tag{41b}$$

The work of Tikhonov is summarized as follows: First, (41b) defines a corresponding slow manifold of the form $y = h(x)$, where $g(x, h(x)) = 0$. Next, let D be the domain over which $h : D \to \mathbb{R}^n$ is continuous. If g and f are sufficiently smooth, then the following theorem provides a more general technical justification for (39):

Theorem 1. *Convergence towards the slow manifold: Suppose the system (40a)–(40b) has an associated slow manifold, $\mathcal{M}_0 = \{(x, y) : y = h(x)\ \&\ x \in D\}$, that is uniformly asymptotically stable. If f, g and their first two derivatives are uniformly bounded in a neighborhood "N" of $\mathcal{M}_0$, then there are positive constants ε_0, b_0, b_1, Λ, and M such that for any initial condition $(x_0, y_0) \in N$ such that $||y_0 - h(x_0)|| \le b_0$, and any ε such that $0 < \varepsilon < \varepsilon_0$, the bound*

$$||y(t) - h(x(t))|| \le M||y_0 - h(x_0)|| \exp[-\Lambda t/\varepsilon] + b_1\varepsilon, \tag{42}$$

holds provided $x(t) \in D$.

Notice the slow manifold utilized in the theorem is not defined to be *invariant*. In fact, $\mathcal{M}_0$ is the nullcline associated with the fast variable, y, and is formally referred to as *the critical manifold*. The non-invariant slow manifold employed in Theorem (1) arises from the original form of the theorem introduced by Tikhonov (1952). The specific form of Theorem (1) is taken directly from Berglund and Gentz (2006), but originally introduced by Gradšteĭn (1953). Fenichel (1979) later extended slow/fast theory by demonstrating that there exists an *invariant* slow manifold that is present in the phase-space of the system when ε is sufficiently small but non-zero.

What the bound specifically tells us is that if $t = \varepsilon|\ln\varepsilon|$, then

$$||y(t) - h(x(t))|| \le M||y_0 - h(x_0)||\varepsilon^\Lambda + b_1\varepsilon, \tag{43}$$

and thus the phase-plane trajectory should be at a distance that is $\mathcal{O}(\varepsilon)$ from $\mathcal{M}_0$ once $t = \varepsilon|\ln\varepsilon|$ (see Berglund and Gentz, 2006, for details). In a fast/slow system of the form (40a)–(40b), the small parameter ε is proportional to the ratio of the fast and slow timescales. Moreover, the system (40a)–(40b) is assumed to be dimensionless. Thus, if we apply Theorem (1) to

$$\begin{aligned} \frac{d\hat{s}_1}{dT} &= (1 + \kappa_1)(1 + \sigma_1)\left[-\hat{s}_1 + (1 - \beta_1)\hat{c}_1\hat{s}_1 + \beta_1\alpha_1\hat{c}_1\right], \\ \varepsilon_2 \frac{d\hat{c}_1}{dT} &= \hat{s}_1 - (1 - \beta_1)\hat{c}_1\hat{s}_1 - \beta_1\hat{c}_1, \end{aligned} \tag{44}$$

then the phase–plane trajectory should be $\mathcal{O}(\varepsilon_2)$ from the c_1-nullcline when $T = \varepsilon_2|\ln\varepsilon_2|$. Consequently, since $T = t/t_{s_1}$, we obtain

$$t = t_{s_1} \cdot \varepsilon_2|\ln\varepsilon_2| = -t_{c_1}\ln\varepsilon_2 \approx t^*_{c_1} \tag{45}$$

as the asymptotic time required for c_1 to reach its maximum value.

The calculation of the matching timescale is more than just an exercise: there is chemical utility in computing $t^*_{c_1}$. Specifically, it indicates approximately when the rate of product formation reaches its maximum quasi-steady-state production:

$$\max \dot{p} \simeq \dot{p}(t^*_{c_1}). \tag{46}$$

Thus, the matching timescale is a very good indication of how long it takes before the product formation rate reaches its maximum value, and when the reaction can be assumed to be in a quasi-steady-state phase.

4. The auxiliary enzyme reaction mechanism

We now consider the more complicated case of the auxiliary enzyme reaction mechanism (Eilertsen and Schnell, 2018). The mechanism is composed of two reactions: a primary reaction (47) that produces a substrate, S_2, that is synthesized in a catalytic step:

$$E_1 + S_1 \underset{k_{-1}}{\overset{k_1}{\rightleftharpoons}} C_1 \overset{k_2}{\to} E_1 + S_2, \tag{47}$$

and a secondary reaction, (48), where S_2 binds with the auxiliary enzyme "E_2" and releases the final product, P:

$$E_2 + S_2 \underset{k_{-3}}{\overset{k_3}{\rightleftharpoons}} C_2 \overset{k_4}{\rightarrow} E_2 + P. \tag{48}$$

The complete set of mass action equations that model the kinetics of the complete reaction mechanism (47)–(48) are

$$\dot{s}_1 = -k_1(e_1^0 - c_1)s_1 + k_{-1}c_1, \tag{49a}$$

$$\dot{c}_1 = k_1(e_1^0 - c_1)s_1 - (k_{-1} + k_2)c_1, \tag{49b}$$

$$\dot{s}_2 = -k_3(e_2^0 - c_2)s_2 + k_{-3}c_2 + k_2c_1, \tag{49c}$$

$$\dot{c}_2 = k_3(e_2^0 - c_2)s_2 - (k_{-3} + k_4)c_2, \tag{49d}$$

where s_1 and s_2 denote the respective concentrations of the substrates S_1 and S_2, c_1 and c_2 denote the concentrations of the complexes C_1 and C_2, and e_1^0 and e_2^0 denote the initial concentrations of the primary and auxiliary enzymes, E_1 and E_2. k_3 and k_{-3} are rate constants, and k_4 is the catalytic constant of the secondary reaction. We define the initial conditions for the secondary reaction as $(s_2, c_2)(t = 0) = (0, 0)$.

In forthcoming analysis, we will assume that the primary reaction obeys the RSA (i.e., $\varepsilon_1 \ll 1$). Additionally, we will make the assumption that $k_2 \lesssim k_4$, and that the initial auxiliary enzyme concentration is larger than e_1^0 (i.e., $e_1^0 = 1,\ e_2^0 \gg 1$). We also compute matching timescales that yield a reliable estimate of the time it takes s_2 and c_2 to reach QSS. Moreover, a new timescale called the *lag time* will be introduced. The lag time corresponds to the time it takes $\dot{p}$ to reach its maximum value, and we will show that it corresponds to a specific matching timescale. Thus, not only do matching timescales provide estimates for the time it takes a specific species to reach QSS, they also, in the context of auxiliary reactions, provide an approximation of the time it takes before the complete reaction begins generating product at a maximal rate.

4.1. The study of phase–plane geometry of the auxiliary enzyme reaction mechanisms permit a heuristic estimation of characteristic timescales

Perhaps the most intuitive way to derive the relevant characteristic timescales of (47)–(48) is to get a qualitative understanding of what a typical phase-plane trajectory looks like in the c_2–s_2 plane. Numerical simulations suggest that the phase–plane trajectory is almost "triangular" in certain parameter ranges (see Fig. 6) and, based on the appearance of the phase–plane trajectory, there seems to be at least three distinct timescales:

- The scale on which the trajectory travels from (a) to (b). We will denote this timescale as t_{s_2}.
- The scale on which the trajectory travels from (b) to (c). We will denote this timescale as t_{c_2}.
- The scale on which the trajectory travels from (c) back to (a). We will denote this timescale as t_p.

The logical step that follows will be to make some initial *a priori* assumptions about the ordering of all the timescales involved in the reaction. For the sake of simplicity, let us initially assume that $t_{c_1} \ll t_{s_2}, t_{c_2} \ll t_{s_1}$, and that the *completion* timescale for the secondary reaction is identically t_{s_1}. This implies that the secondary reaction completes at roughly the same time as the primary reaction, and that $t_p \approx t_{s_1}$. Thus, we have eliminated one timescale (t_p)

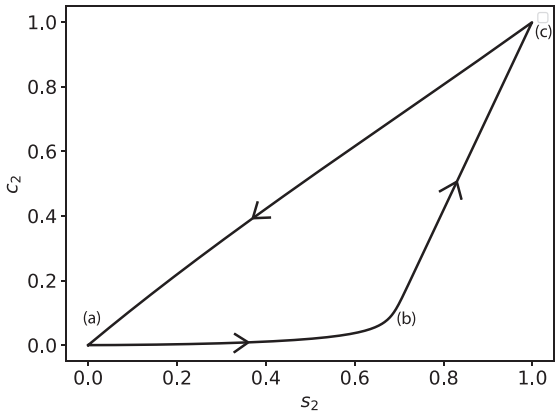

Fig. 6. The phase–plane portrait of the mass action trajectory for the auxiliary reaction mechanism (47)–(48). The solid black curve is the numerically-computed solution to (49a)–(49d). The initial concentrations and rate constants used in the numerical simulation are: $k_1 = 1,\ k_2 = 1,\ k_{-1} = 1,\ e_1^0 = 1,\ e_2^0 = 100,\ k_{-3} = 1,\ k_3 = 1,\ k_4 = 2$ and $s_1^0 = 100$ (units have been omitted). s_2 and c_2 have been scaled by their numerically obtained maximum values.

by imposing the assumption that the secondary reaction is as fast as the primary reaction.

The next step will be to exploit the presence and geometry of any manifolds (not necessarily invariant) that exist within the phase-plane of the secondary reaction. Notice that the intersection of the s_2-nullcline and c_2-nullcline is *time-dependent* since the s_2-nullcline moves as c_1 varies in time. Geometrically, the intersection of the nullclines is described by a moving fixed point, $\boldsymbol{x}^*$,

$$N_{s_2} \cap N_{c_2} \equiv \boldsymbol{x}^*, \tag{50}$$

where N_{s_2} denotes the s_2-nullcline and N_{c_2} denotes the c_2-nullcline. Algebraically, the coordinates of $\boldsymbol{x}^*$, (s_2^*, c_2^*), are

$$s_2^* = \frac{K_{M_2}k_2c_1(t)}{V_2 - k_2c_1(t)}, \quad c_2^* = \frac{k_2c_1(t)}{k_4}, \tag{51}$$

where K_{M_2} denotes the Michaelis constant of the secondary reaction

$$K_{M_2} \equiv \frac{k_{-3} + k_4}{k_3}, \tag{52}$$

and V_2 denotes the limiting rate of the secondary reaction: $V_2 \equiv k_4e_2^0$. Moreover, if the second reaction is as fast as the primary reaction, then the phase-plane geometry suggests that the trajectory should not only catch the fixed point $\boldsymbol{x}^*$, but will also approximately *adhere* to $\boldsymbol{x}^*$ as it descends to the origin. If the trajectory adheres to $\boldsymbol{x}^*$, then

$$\dot{p} = \frac{V_2\dfrac{K_{M_2}k_2c_1}{V_2 - k_2c_1}}{K_{M_2} + \dfrac{K_{M_2}k_2c_1}{V_2 - k_2c_1}} = k_2c_1, \tag{53}$$

and the product formation rate of the secondary reaction has reached its limiting value. Notice that by assuming that the secondary reaction is fast enough to virtually adhere to $\boldsymbol{x}^*$ implies $V_2 > k_2c_1^{\max}$. Thus, this assumption admits an automatic partition of parameter space, and we will only consider regions of parameter space within which $V_2 > k_2c_1^{\max} = k_2\varepsilon_1 s_1^0$ holds.

Since the position of the s_2-nullcline depends on the concentration c_1, we want to estimate how c_1 varies over the course of the reaction. Since we are assuming that the primary reaction follows the RSA, the phase-plane trajectory will closely follow a slow manifold when $t \geq t_{c_1}^*$. If we know the shape of the slow manifold, then we can get a rough idea of how c_1 varies throughout the reaction.

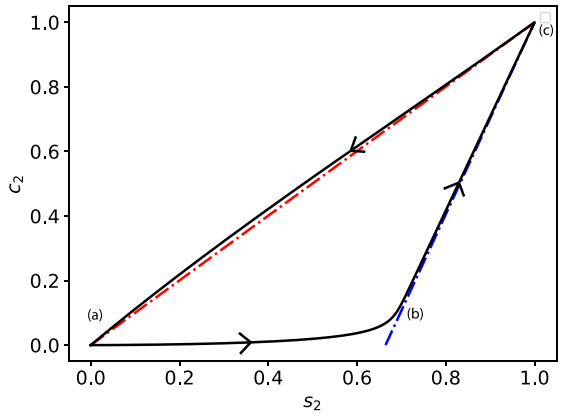

Fig. 7. The s_2–c_2 phase-plane trajectory (with nullclines) for the auxiliary reaction mechanism (47)–(48). The thick black curve is the numerically-integrated solutions to the mass action Eqs. (49a)–Eqs. (49d). The broken red curve is the c_2-nullcline, and the broken blue curve is the fixed s_2-nullcline ($N_{s_2}^{\max}$, given by (56)). The phase–plane trajectory initially moves towards $N_{s_2}^{\max}$, then moves up $N_{s_2}^{\max}$ before moving back down the c_2-nullcline. The constants (without units) used in the numerical simulation are: $e_1^0 = 1$, $s_1^0 = 1000$, $k_1 = 1$, $k_2 = 1$, $k_3 = 1$, $k_{-3} = 1$, $k_4 = 2$, $e_2^0 = 100$ and $k_{-1} = 1$. Curves were scaled by their numerically obtained maximum values. (For interpretation of the references to colour in this figure legend, the reader is referred to the web version of this article.)

To do this, we will look at the dimensionless equations

$$\frac{d\hat{s}_1}{dT} = (1+\kappa_1)(1+\sigma_1)\left[-\hat{s}_1 + (1-\beta_1)\hat{c}_1\hat{s}_1 + \beta_1\alpha_1\hat{c}_1\right],$$
$$\varepsilon_2\frac{d\hat{c}_1}{dT} = \hat{s}_1 - (1-\beta_1)\hat{c}_1\hat{s}_1 - \beta_1\hat{c}_1. \tag{54}$$

The zeroth order asymptotic approximation to the slow manifold is the $\hat{c}_1$-nullcline:

$$\hat{s}_1 - (1-\beta_1)\hat{c}_1\hat{s}_1 - \beta_1\hat{c}_1 = 0. \tag{55}$$

Notice that $\beta_1 \to 0$ as $\sigma_1 \to \infty$; thus, as $\sigma_1 \to \infty$, the trajectory that follows the slow manifold will be asymptotic to the curve $\hat{c}_1 = 1$ for most of the reaction. Hence, when $\sigma_1 \gg 1$, the concentration of the intermediate complex remains near its maximum value, $c_1^{\max}$, for the majority of the reaction, and the s_2-nullcline will be effectively stationary after the initial buildup of c_1. Under the assumption that t_{c_1} is the shortest timescale, the initial transient behavior of c_2 will occur while the s_2-nullcline remains fixed. Thus, we look at the phase–plane trajectory with the s_2-nullcline (with fixed c_1) at its stationary value (see Fig. 7). Let us denote this manifold as $N_{s_2}^{\max}$:

$$N_{s_2}^{\max} \equiv \left\{(s_2, c_2) \in \mathbb{R}^2 : c_2 - \frac{k_3 e_2^0 s_2 - k_2 c_1^{\max}}{k_3 s_2 + k_{-3}} = 0\right\}. \tag{56}$$

Next, we want to exploit the phase-plane geometry in order to estimate critical timescales. We will first estimate t_{s_2} by noting that the phase–plane trajectory essentially lies along the s_2–axis for $t \le t_{s_2}$. This suggests that

$$\dot{s}_2 \approx -k_3 s_2 + k_2 c_1, \quad t \le t_{s_2} \tag{57}$$

is a reasonable approximation to (49c). If the initial fast transient of the primary reaction is negligibly short, i.e., $t_{c_1} \ll t_{s_2}$, then it is reasonable to assume

$$\dot{s}_2 \approx -k_3 s_2 + k_2 c_1^{\max}, \quad t \le t_{s_2}. \tag{58}$$

Since (58) is linear, its exact solution

$$s_2 \approx s_2^{\lambda}[1 - \exp(-t/t_{s_2})] \tag{59}$$

provides two critical estimates: the characteristic timescale, t_{s_2}, and an approximate maximum value of s_2 on the t_{s_2} timescale:

$$t_{s_2} \equiv \frac{1}{k_3 e_2^0}, \quad s_2 \le s_2^{\lambda} \equiv \frac{k_2 c_1^{\max}}{k_3 e_2^0}. \tag{60}$$

The prediction that $s_2 < s_2^{\max}$ for $t \le t_{s_2}$ (obtained from the linear equation) is in qualitative agreement with the phase-plane trajectory of the numerically-integrated equations (Fig. 7).

Next, to estimate t_{c_2}, we note that since the phase–plane trajectory lies close to $N_{s_2}^{\max}$ along its ascension to $c_2^{\max}$, the growth of the intermediate complex is approximately

$$\dot{c}_2 \approx -k_4 c_2 + k_2 c_1^{\max}, \quad t_{s_2} \le t \le t_{c_2}, \tag{61}$$

which admits an analytical solution:

$$c_2 \approx c_2^{\max}[1 - \exp(-k_4 t)]. \tag{62}$$

Trajectories that follow the s_2-nullcline closely are said to be in rapid equilibrium (Nguyen and Fraser, 1989; Roussel and Fraser, 1991) or a reverse quasi-steady-state (Schnell and Maini, 2000). This is in contrast to trajectories that follow the c_2-nullcline, which are said to be in a quasi-steady-state phase (Eilertsen and Schnell, 2018). From (62), we have two observations: (i) k_4^{-1} is a reasonable estimate of t_{c_2}, and (ii) this linearized solution predicts c_2 will approach $c_2^{\max}$, which is in qualitative agreement with the phase–plane trajectory.

As a concluding remark of this subsection, we note that there are four timescales, $t_{c_1}, t_{s_2}, t_{c_2}$ and t_{s_1}, that influence the overall dynamics of the coupled reaction. Only two timescales are needed to characterize the dynamics of the single-enzyme, single-substrate MM reaction mechanism. Thus, only the ordering of two timescales, t_{c_1} and t_{s_1}, needs to be considered. In the case of the coupled reaction, there are multiple orderings that need to be considered in order to fully comprehend the dynamics. In the immediate subsections that follow, we will analyze the dynamics with respect to the orderings: $t_{c_1} \ll t_{s_2} \ll t_{c_2} \ll t_{s_1}$ and $t_{s_2}, t_{c_2} \ll t_{c_1} \ll t_{s_1}$. Both analyses of these orderings will be made under the assumption that e_2^0 is large with respect to e_1^0.

4.2. Scaling analysis: $t_{c_1} \ll t_{s_2} \ll t_{c_2} \ll t_{s_2}$

Although we now have estimates for the timescales t_{s_2} and t_{c_2}, it is important to remember that these timescales were obtained under the assumption that c_1 is the fastest variable (i.e., c_1 reaches its maximum before any other variable). We must now: (i) determine the appropriate conditions under which approximate adhesion to $\boldsymbol{x}^*$ is possible, and (ii) determine the onset of validity for (53). We begin by scaling the mass action equations. Introducing the additional scaled concentrations

$$\hat{s}_2 = s_2/s_2^{\max}, \quad \hat{c}_2 = c_2/c_2^{\max} \tag{63}$$

into Eqs. (49c)–Eqs. (49d) admits the dimensionless form:

$$\frac{d\hat{s}_1}{dT} = (1+\kappa_1)(1+\sigma_1)\left[-\hat{s}_1 + (1-\beta_1)\hat{c}_1\hat{s}_1 + \beta_1\alpha_1\hat{c}_1\right], \tag{64a}$$

$$\varepsilon_2\frac{d\hat{c}_1}{dT} = \hat{s}_1 - (1-\beta_1)\hat{c}_1\hat{s}_1 - \beta_1\hat{c}_1 \tag{64b}$$

$$\mu_1\frac{d\hat{s}_2}{dT} = -\hat{s}_2 + (1-\beta_2)\hat{s}_2\hat{s}_2 + \beta_2\alpha_2\hat{c}_2 + r_S\mu_1\hat{c}_1, \tag{64c}$$

$$\mu_2\frac{d\hat{c}_2}{dT} = (1+\kappa_2)(1+\sigma_2)\left[(\hat{s}_2 - (1-\beta_2)\hat{c}_2\hat{s}_2 - \beta_2\hat{c}_2\right]. \tag{64d}$$

The dimensionless parameters κ_2, σ_2, and r_S, introduced in (64a)–(64d), are

$$\alpha_2 \equiv \frac{\kappa_2}{1+\kappa_2}, \quad \beta_2 \equiv \frac{1}{1+\sigma_2}, \quad \kappa_2 \equiv \frac{k_{-3}}{k_4}, \quad \sigma_2 \equiv \frac{s_2^{\max}}{K_{M_2}}, \quad r_S \equiv \frac{s_1^0}{s_2^{\max}}. \tag{65}$$

The remaining parameters, μ_1 and μ_2, are the ratios of the secondary reaction timescales to the primary reaction substrate timescale:

$$\mu_1 \equiv \frac{t_{s_2}}{t_{s_1}}, \quad \mu_2 \equiv \frac{t_{c_2}}{t_{s_1}}. \tag{66}$$

It follows from (66) that if $\{\varepsilon_2, \mu_1, \mu_2\} \ll 1$, then the dynamics of (49a)–(49d) consist of one slow variable, s_1, and three fast variables: c_1, s_2 and c_2. The designation of s_1 as a slow variable and c_1, s_2 and c_2 as fast variables implies that after an initial fast transient, the phase–plane trajectory is asymptotic to the intersecting nullclines:

$$s_2 \simeq \frac{K_{M_1}}{V_2 - k_2 c_1} k_2 c_1, \tag{67a}$$

$$c_2 \simeq \frac{k_2 c_1}{k_4}. \tag{67b}$$

After the initial fast transient of the primary reaction, $k_2 c_1$ is asymptotic to

$$k_2 c_1 \simeq \frac{V_1}{K_{M_1} + s_1} s_1 \equiv -\dot{s}_1^{\varepsilon}, \tag{68}$$

and thus c_1, s_2 and c_2 are, in the asymptotic limit, explicitly dependent on s_1 only.

The above approximations, (67a)–(67b), confirm the hypothesis that the phase-plane trajectory follows the intersection of the s_2- and c_2-nullclines as long as the secondary reaction is fast (i.e., μ_1, $\mu_2 \ll 1$). The additional assumption made in the derivation of t_{s_2} and t_{c_2} was that t_{c_1} is the *shortest* timescale, and that there is no significant formation of s_2 or c_2 for $0 \le t \le t_{c_1}$. To assess the validity of this assumption, we rescale (49c)–(49d) with respect to $\tau = t/t_{c_1}$:

$$\frac{d\hat{s}_1}{d\tau} = \varepsilon_1 \left[-\hat{s}_1 + (1-\beta_1)\hat{c}_1\hat{s}_1 + \beta_1\alpha_1\hat{c}_1 \right], \tag{69a}$$

$$\frac{d\hat{c}_1}{d\tau} = \left[\hat{s}_1 - (1-\beta_1)\hat{c}_1\hat{s}_1 - \beta_1\hat{c}_1 \right] \tag{69b}$$

$$\frac{d\hat{s}_2}{d\tau} = \lambda_1 \left[-\hat{s}_2 + (1-\beta_2)\hat{c}_2\hat{s}_2 + \beta_2\alpha_2\hat{c}_2 \right] + r_S\varepsilon_2\hat{c}_1, \tag{69c}$$

$$\frac{d\hat{c}_2}{d\tau} = \lambda_2(1+\kappa_2)(1+\sigma_2)\left[\hat{s}_2 - (1-\beta_2)\hat{c}_2\hat{s}_2 - \beta_2\hat{c}_2 \right]. \tag{69d}$$

The parameters that emerge from scaling, λ_1 and λ_2, are the ratios we need in order to calculate the time that transpires before (67a)–(67b) become valid approximations:

$$\lambda_1 = \frac{t_{c_1}}{t_{s_2}}, \quad \lambda_2 = \frac{t_{c_1}}{t_{c_2}}. \tag{70}$$

It is straightforward to show that the term "$r_S\varepsilon_2$" in (69c) is bounded above,

$$r_S\varepsilon_2 < \lambda_1, \tag{71}$$

and therefore s_2 is slow on t_{c_1} when $\lambda_1 \ll 1$. In addition, (69d) implies that $\lambda_2(1+\kappa_2)(1+\sigma_2) \ll 1$ if c_2 is to be *slow* over t_{c_1}. While it is certainly true that $\lambda_2(1+\kappa_2)(1+\sigma_2) \ll 1$ is sufficient for c_2 to be slow, it is not necessary, given that $s_2 \simeq 0$ for $t \le t_{c_1}$.

Piecing together the results obtained from the scaling analysis, we obtain

$$s_1 \simeq s_1^0, \tag{72a}$$

$$c_1 \simeq c_1^{\max}[1 - \exp(-t/t_{c_1})], \tag{72b}$$

$$s_2 \simeq 0, \tag{72c}$$

$$c_2 \simeq 0, \tag{72d}$$

for $t \lesssim t_{c_1}$.

Moving forward, the next "fastest" timescale in our imposed ordering is t_{s_2}. We note that in addition to c_2 scaling as a slow variable over t_{c_1}, the phase-plane trajectory indicates that c_2 will also be slow over t_{s_2}. Thus, we rescale the complete set of mass action equations with respect to $\bar{T} = t/t_{s_2}, \tilde{s}_2 = s_2/s_2^{\lambda}$ and $\tilde{c}_2 = c_2/e_2^0 s_2^{\lambda}/(K_{M_2} + s_2^{\lambda})$:

$$\frac{d\hat{s}_1}{d\bar{T}} = \mu_1(1+\kappa_1)(1+\sigma_1)\left[-\hat{s}_1 + (1-\beta_1)\hat{c}_1\hat{s}_1 + \beta_1\alpha_1\hat{c}_1 \right], \tag{73a}$$

$$\varepsilon_1\frac{d\hat{c}_1}{d\bar{T}} = \mu_1(1+\kappa_1)(1+\sigma_1)\left[\hat{s}_1 - (1-\beta_1)\hat{c}_1\hat{s}_1 - \beta_1\hat{c}_1 \right] \tag{73b}$$

$$\frac{d\tilde{s}_2}{d\bar{T}} = -\tilde{s}_2 + (1-\tilde{\beta}_2)\tilde{c}_2\tilde{s}_2 + \tilde{\beta}_2\alpha_2\tilde{c}_2 + \hat{c}_1, \tag{73c}$$

$$\frac{d\tilde{c}_2}{d\bar{T}} = \nu(1+\kappa_2)(1+\tilde{\sigma}_2)\left[\tilde{s}_2 - (1-\tilde{\beta}_2)\tilde{c}_2\tilde{s}_2 - \tilde{\beta}_2\tilde{c}_2 \right]. \tag{73d}$$

In (73c), the dimensionless parameters $\tilde{\sigma}_2$ and $\tilde{\beta}_2$ are given by:

$$\tilde{\sigma}_2 \equiv \frac{s_2^{\lambda}}{K_{M_2}}, \quad \tilde{\beta}_2 = \frac{1}{1+\tilde{\sigma}_2} \tag{74}$$

Consequently, the production of s_2 will be significant on t_{s_2}. From (73d), we see that if $\nu(1+\kappa_2)(1+\tilde{\sigma}_2) \ll 1$, *where* $\nu = \frac{t_{s_2}}{t_{c_2}}$, then c_2 will be a slow variable with respect to the t_{c_1} timescale. In fact, it is worth pointing out that

$$[\nu(1+\kappa_2)(1+\sigma_2)]^{-1} = \frac{e_2^0}{K_{M_2} + s_2^{\max}} \equiv \epsilon, \tag{75}$$

which is the analogue of ε_1 for the secondary reaction. Thus, the scaling analysis indicates that c_2 will be a slow variable over t_{s_2} if $\epsilon \gg 1$, which suggests e_2^0 should be large in comparison to $K_{M_2} + s_2^{\max}$.

Next, we see from (73b) that

$$\frac{\varepsilon_1\mu_1^{-1}}{(1+\kappa_1)(1+\sigma_1)} = \frac{t_{c_1}}{t_{s_2}}, \tag{76}$$

and thus c_1 will be in QSS on the t_{s_2} timescale as long as $t_{c_1} \ll t_{s_2}$.

From Eq. (73a), it is clear that if $\mu_1(1+\kappa_1)(1+\sigma_1) \ll 1$, then s_1 will be a slow variable over the t_{s_2} timescale. However, this condition is sufficient but not necessary; since c_1 is in QSS, we have:

$$\dot{s}_1 \simeq -\frac{V_1}{K_{M_1} + s_1} s_1. \tag{77}$$

If we then rescale (77) with respect to $\bar{T}$, we obtain:

$$\frac{d\hat{s}_1}{d\bar{T}} \simeq -\mu_1\frac{\hat{s}_1(1+\sigma_1)}{1+\sigma_1\hat{s}_1} \ge -\mu_1. \tag{78}$$

Thus, given (78), we see that if $\mu_1 \ll 1$ is both necessary *and* sufficient for s_1 to be a slow variable with respect t_{s_2} when c_1 is in QSS. Assuming this condition is met, and the RSA holds, we obtain

$$s_1 \simeq s_1^0, \tag{79a}$$

$$c_1 \simeq c_1^{\max}, \tag{79b}$$

$$s_2 \simeq s_2^{\lambda}[1-\exp(-t/t_{s_2})], \tag{79c}$$

$$c_2 \simeq 0, \tag{79d}$$

for $t_{c_1} \lesssim t \lesssim t_{s_2}$.

The remaining dimensionless timescale necessary for the completion of the scaling analysis is $\bar{\tau} = t/t_{c_2}$. Rescaling yields

$$\frac{d\hat{s}_1}{d\bar{\tau}} = \mu_2(1+\kappa_1)(1+\sigma_1)\left[-\hat{s}_1 + (1-\beta_1)\hat{c}_1\hat{s}_1 + \beta_1\alpha_1\hat{c}_1\right], \tag{80a}$$

$$\varpi\frac{d\hat{c}_1}{d\bar{\tau}} = \hat{s}_1 - (1-\beta_1)\hat{c}_1\hat{s}_1 - \beta_1\hat{c}_1, \tag{80b}$$

$$\nu\frac{d\hat{s}_2}{d\bar{\tau}} = -\hat{s}_2 + (1-\beta_2)\hat{c}_2\hat{s}_2 + \beta_2\alpha_2\hat{c}_2 + r_S\mu_1\hat{c}_1, \tag{80c}$$

$$\frac{d\hat{c}_2}{d\bar{\tau}} = (1+\kappa_2)(1+\sigma_2)\left[\hat{s}_2 - (1-\beta_2)\hat{c}_2\hat{s}_2 - \beta_2\hat{c}_2\right], \tag{80d}$$

where $\varpi = t_{c_1}/t_{c_2}$. Again, if $\varpi \ll 1$, then c_1 is in QSS, in which case

$$\frac{d\hat{s}_1}{d\bar{\tau}} \simeq -\mu_2\frac{\hat{s}_1(1+\sigma_1)}{1+\sigma_1\hat{s}_1} \geq -\mu_2, \tag{81}$$

and s_1 is a slow variable with respect to t_{c_2}.

Next, if $\nu \ll 1$, then s_2 is in QSS on the t_{c_2} timescale, which implies

$$s_2 \simeq \frac{k_{-3}c_2 + k_2c_1^{\max}}{k_3(e_2^0 - c_2)}, \quad \therefore \quad s_2^{\lambda} \leq s_2 \leq s_2^{\max}. \tag{82}$$

Thus, the scaling analysis indicates that

$$s_1 \simeq s_1^0, \tag{83a}$$

$$c_1 \simeq c_1^{\max}, \tag{83b}$$

$$s_2 \simeq \frac{k_{-3}c_2 + k_2c_1^{\max}}{k_3(e_2^0 - c_2)}, \tag{83c}$$

$$c_2 \simeq c_2^{\max}[1-\exp(-t/t_{c_2})], \tag{83d}$$

for $t_{s_2} \lesssim t \lesssim t_{c_2}$, and the results of the complete scaling analysis allow us to formally construct the composite solutions for s_2 and c_2:

$$s_2^{io} = -s_2^{\lambda}[\exp(-t/t_{s_2})] + \frac{k_{-3}c_2^{io} + k_2c_1^{\max}}{k_3(e_2^0 - c_2^{io})} - \frac{K_{M_2}}{V_2 + \dot{s}_1^{\varepsilon}}\dot{s}_1^{\varepsilon} - s_2^{\max}, \tag{84a}$$

$$c_2^{io} = -c_2^{\max}[\exp(-t/t_{c_2})] - \dot{s}_1^{\varepsilon}/k_4. \tag{84b}$$

Together, (84a) and (84b) provide a uniform asymptotic expansion that is valid for all time (see Fig. 8).

4.3. The lag time appears when there are multiple layers and multiple matching timescales

In the previous subsection, we derived inner (initial fast transient) and outer (quasi-steady-state phase) solutions that are valid when $t_{c_1} \ll t_{s_2} \ll t_{c_2} \ll t_{s_1}$. Formally, the ordering, $t_{c_1} \ll t_{s_2} \ll t_{c_2} \ll t_{s_1}$, categorizes t_{c_1} as a *super-fast* timescale, t_{s_2} as a *fast* timescale, t_{c_2} as a *slow* timescale, and t_{s_1} as a *super-slow* timescale. From a theoretical perspective, there is utility in estimating the time it takes for s_2 and c_2 to reach $\boldsymbol{x}^*$, at which time the rate of product formation, $\dot{p}$, is at its maximum value. Let $t_{s_2}^*$ denote the actual time it takes s_2 to reach s_2^*, and let $t_{c_2}^*$ denote the actual time it takes s_2 and c_2 to reach $\boldsymbol{x}^*$. Since t_{s_2} and t_{c_2} are characteristic timescales, utilizing them as *matching* timescales is problematic since the transition regimes, $t_{s_2} \leq t \leq t_{s_2}^*$ and $t_{c_2} \leq t \leq t_{c_2}^*$, can be quite large. Thus, what we seek are reliable estimates for $t_{s_2}^*$ and $t_{c_2}^*$. To construct these estimates, we will utilize the approximation techniques introduced in Section 3. Starting with $t_{c_2}^*$, the inner solution for the formation of c_2 is

$$c_2 \simeq c_2^{\max}[1-\exp(-t/t_{c_2})]. \tag{85}$$

Although t_{c_2} is a slow timescale, it is fast with respect to t_{s_1}. Thus, rewriting (85) with respect to T yields

$$c_2 \simeq c_2^{\max}[1-\exp(-T/\mu_2)], \tag{86}$$

and we see that $T = \mu_2|\ln\mu_2|$ provides an estimate for $t_{c_2}^*$:

$$t_{c_2}^* \approx -t_{c_2}\ln\mu_2. \tag{87}$$

The estimate given in (87) is the approximate time it takes for $\dot{p}$ to reach it maximum with respect to the timescale ordering $t_{c_1} \ll t_{s_2} \ll t_{c_2} \ll t_{s_1}$ (see Fig. 9). Formally, the matching timescale $t_{c_2}^*$ is the lag time, or the time during which the second reaction "lags" behind the first reaction.

Next we estimate the matching timescale $t_{s_2}^*$, which is roughly the time it takes for s_2 to reach QSS. The inner solution

$$s_2 \simeq s_2^{\lambda}[1-\exp(-t/t_{s_2})], \tag{88}$$

can be expressed in terms of its corresponding slow timescale $\bar{\tau}$:

$$s_2 \simeq s_2^{\lambda}[1-\exp(-\bar{\tau}/\nu)]. \tag{89}$$

Employing a direct method yields

$$t_{s_2}^* \approx -t_{s_2}\ln\nu, \tag{90}$$

which we take as our approximation to the matching timescale $t_{s_2}^*$.

In addition to the estimate (90) obtained by the direct method, we can employ scaling and justify both (90) and (87) by invoking Theorem 1. The scaled mass action Eqs. (64a)–(64d), can be systematically reduced on the super-slow timescale (i.e., $T = t/t_{s_1}$). Since ε_2 and μ_1 are, respectively, the smallest parameters with respect to the ordering $t_{c_1} \ll t_{s_2} \ll t_{c_2} \ll t_{s_1}$, we can write

$$\frac{d\hat{s}_1}{dT} = -\frac{\hat{s}_1(\sigma_1+1)}{1+\sigma_1\hat{s}_1} + \mathcal{O}(\varepsilon_2), \tag{91a}$$

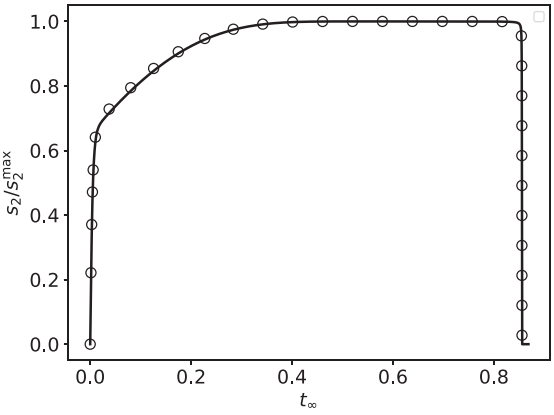

Fig. 8. A graphical illustration of the accuracy of the composite solutions for the auxiliary reaction mechanism (47)–(48). The solid black curve is the numerical solution to (49c), and the unfilled circles mark the composite solution (84a). The constants (without units) used in the numerical simulation are: $e_1^0 = 1$, $s_1^0 = 1000$, $e_2^0 = 100$, $k_1 = 1$, $k_2 = 1$, $k_3 = 1$, $k_{-3} = 1$, $k_4 = 2$ and $k_{-1} = 1$. Time has been mapped to the t_∞ scale: $t_\infty(t) = 1 - 1/\ln[t + \exp(1)]$. The substrate concentration has been scaled by its maximum value.

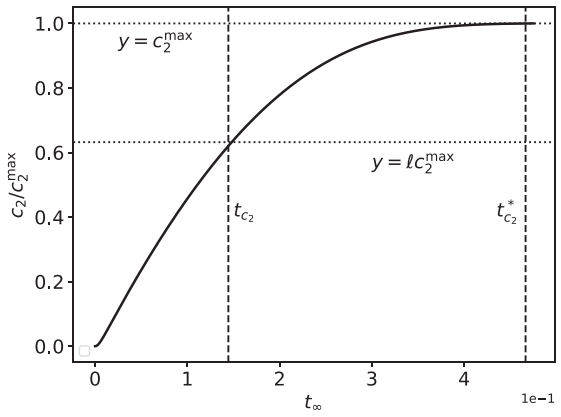

Fig. 9. The timescale t_{c_2} is characteristic of the time it takes c_2 to reach $c_2^{\max}$, and the timescale $t^*_{c_2}$ is the approximate time it takes c_2 to reach $c_2^{\max}$, respectively, in the auxiliary reaction mechanism (47)–(48). The thick black curve is the numerically-integrated solutions to the mass action Eqs. (49a)–(49d). The leftmost dashed vertical line corresponds to t_{c_2}, and the rightmost dashed vertical line corresponds to $t^*_{c_2} = -t_{c_2}\ln t_{c_2}/t_{s_1}$. The lower dotted horizontal line corresponds to the scaled characteristic value $\ell c_2^{\max}$, and the upper dotted horizontal line corresponds to $c_2^{\max}$. The constants (without units) used in the numerical simulation are: $e_1^0 = 1$, $s_1^0 = 1000$, $e_2^0 = 100$, $k_1 = 1$, $k_2 = 1$, $k_3 = 1$, $k_{-3} = 1$, $k_4 = 2$ and $k_{-1} = 1$. Time has been mapped to the t_∞ scale: $t_\infty(t) = 1 - 1/\ln[t + \exp(1)]$, and c_2 has been numerically scaled by its maximum value. Note that the mass action equations have only been integrated from $t = 0$ to $t \approx t^*_{c_2}$ for clarity.

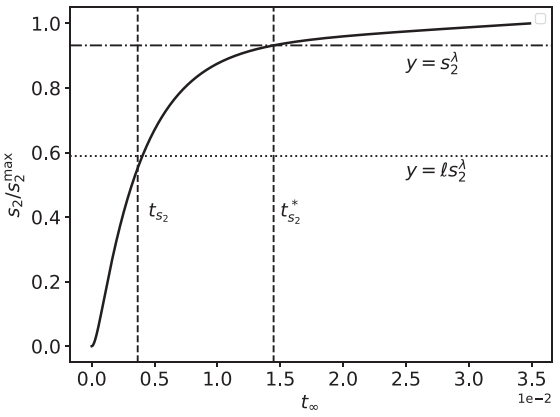

Fig. 10. The timescale t_{s_2} is characteristic of the time it takes s_2 to reach s_2^λ, and the timescale $t^*_{s_2}$ is the approximate time it takes s_2 to reach s_2^λ, respectively, in the auxiliary reaction mechanism (47)–(48). The thick black curve is the numerically-integrated solution to the mass action Eqs. (49a)–(49d). The leftmost dashed vertical line corresponds to t_{s_2}, and the rightmost dashed vertical line corresponds to $t^*_{s_2} = -t_{s_2}\ln t_{s_2}/t_{c_2}$. The lower dotted horizontal line corresponds to the scaled characteristic value ℓs_2^λ, and the upper dashed/dotted vertical line corresponds to s_2^λ. The constants (without units) used in the numerical simulation are: $e_1^0 = 1$, $s_1^0 = 1000$, $e_2^0 = 100$, $k_1 = 1$, $k_2 = 1$, $k_3 = 1$, $k_{-3} = 1$, $k_4 = 2$ and $k_{-1} = 1$. Time has been mapped to the t_∞ scale: $t_\infty(t) = 1 - 1/\ln[t + \exp(1)]$, and s_2 has been numerically-scaled by its maximum value. For clarity, the mass action equations have been integrated from $t = 0$ to $t \approx t^*_{s_2}$.

$$\mu_2 \frac{d\hat{c}_2}{dT} = \frac{\hat{s}_1(\sigma_1 + 1)}{1 + \sigma_1 \hat{s}_1} - \hat{c}_2 + \mathcal{O}(\varepsilon_2, \mu_1), \tag{91b}$$

which are the scaled, leading-order asymptotic equations on the T-timescale. Applying Theorem 1 to (91a)–(91b) suggests that c_2 should approximately reach QSS when $T \approx \mu_2|\ln \mu_2|$.

Alternatively, by looking carefully at the scaling obtained with respect to $\bar{\tau}$, the leading order dynamics are given by:

$$\nu \frac{d\hat{s}_2}{d\bar{\tau}} = \left[-\hat{s}_2 + (1 - \beta_2)\hat{c}_2\hat{s}_2 + \beta_2\alpha_2\hat{c}_2\right] + r_S\mu_1[1 + \mathcal{O}(\mu_2, \varepsilon_1)], \tag{92a}$$

$$\frac{d\hat{c}_2}{d\bar{\tau}} = (1 + \kappa_2)(1 + \sigma_2)\left[\hat{s}_2 - (1 - \beta_2)\hat{c}_2\hat{s}_2 - \beta_2\hat{c}_2\right]. \tag{92b}$$

Pursuant to Theorem 1, (92a)–(92b) indicate s_2 should reach QSS when $\bar{\tau} \approx \nu|\ln \nu|$; consequently, we take

$$t^*_{s_2} \approx -t_{s_2}\ln \nu, \tag{93}$$

as the asymptotic estimate (i.e., the matching timescale) of the time it takes for s_2 to reach QSS (see Fig. 10).

4.4. Scaling analysis: $t_{s_2}, t_{c_2} \ll t_{c_1} \ll t_{s_1}$

In the most extreme case, when both t_{s_2} and t_{c_2} are much less than t_{c_1} in magnitude, scaling analysis indicates that both s_2 and c_2 are fast variables over both the τ and T timescales:

$$\frac{d\hat{s}_1}{d\tau} = \varepsilon_1\left[-\hat{s}_1 + (1 - \beta_1)\hat{c}_1\hat{s}_1 + \beta_1\alpha_1\hat{c}_1\right], \tag{94a}$$

$$\frac{d\hat{c}_1}{d\tau} = \left[\hat{s}_1 - (1 - \beta_1)\hat{c}_1\hat{s}_1 - \beta_1\hat{c}_1\right], \tag{94b}$$

$$\lambda_1^{-1}\frac{d\hat{s}_2}{d\tau} = \left[-\hat{s}_2 + (1 - \beta_2)\hat{c}_2\hat{s}_2 + \beta_2\alpha_2\hat{c}_2\right] + r_S\mu_1\hat{c}_1, \tag{94c}$$

$$\lambda_2^{-1}\frac{d\hat{c}_2}{d\tau} = (1 + \kappa_2)(1 + \sigma_2)\left[\hat{s}_2 - (1 - \beta_2)\hat{c}_2\hat{s}_2 - \beta_2\hat{c}_2\right]. \tag{94d}$$

Recall that $\lambda_1 \equiv t_{c_1}/t_{s_2}$ and $\lambda_2 \equiv t_{c_1}/t_{c_2}$, and that λ_1^{-1} and λ_2^{-1} will be small when t_{s_2} and t_{c_2} are *super-fast* timescales, t_{c_1} is a *fast* timescale, and t_{s_1} is a *slow* timescale. Consequently, both s_2 and c_2 are given in terms of c_1

$$s_2 \simeq \frac{K_{M_2}k_2c_1}{V_2 - k_2c_1}, \tag{95a}$$

$$c_2 \simeq \frac{k_2c_1}{k_4}, \tag{95b}$$

for $t \geq 0$. Since the secondary reaction is asymptotically determined by c_1 when $t_{s_2}, t_{c_2} \ll t_{c_1} \ll t_{s_1}$, the production rate will reach a maximum when $t \approx t^*_{c_1}$ (see Fig. 11). Thus, the matching timescale $t^*_{c_1}$ is synonymous with time it takes for $\dot{p}$ to reach its maximum value.

5. Alternative orderings of timescale for the auxiliary enzyme reaction

The previous sections and subsections dealt primarily with the ordering $t_{c_1} \ll t_{s_2} \ll t_{c_2} \ll t_{s_1}$. It is natural to ask what happens when this ordering starts to change, and in this section we will briefly analyze the dynamics of (48) in regimes where the ordering, $t_{c_1} \ll t_{s_2} \ll t_{c_2} \ll t_{s_1}$, is no longer preserved.

5.1. Scaling analysis for $t_{c_1} \ll t_{c_2} \ll t_{s_2} \ll t_{s_1}$: A three versus four timescale perspective

The first ordering we consider is that in which t_{c_1} is a *super-fast* timescale, t_{c_2} is a fast timescale, t_{s_2} is a slow timescale, and t_{s_1} is *super-slow* timescale: $t_{c_1} \ll t_{c_2} \ll t_{s_2} \ll t_{s_1}$. We will start the analysis by observing the scaling with respect to $\bar{\tau}$:

$$\frac{d\hat{s}_1}{d\bar{\tau}} = \mu_2(1 + \kappa_1)(1 + \sigma_1)\left[-\hat{s}_1 + (1 - \beta_1)\hat{c}_1\hat{s}_1 + \beta_1\alpha_1\hat{c}_1\right], \tag{96a}$$

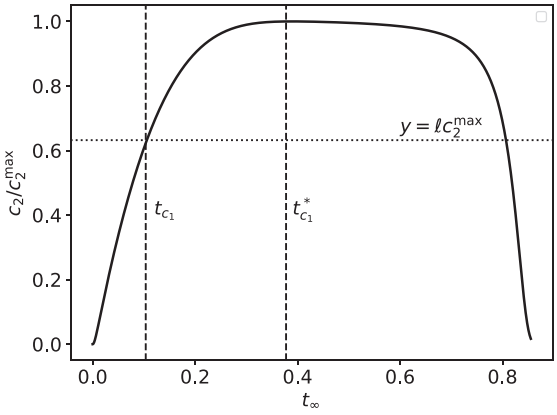

Fig. 11. When $t_{c_2}, t_{s_2} \ll t_{c_1}$, the timescale t_{c_1} is characteristic of the time it takes $\dot{p}$ to reach its maximum, and the timescale $t^*_{c_1}$ is the approximate time it takes c_2 to reach its maximum, respectively, in the auxiliary reaction mechanism (47)–(48). The thick black curve is the numerically-integrated solution to the mass action Eqs. (49a)–(49d). The leftmost dashed vertical line corresponds to t_{c_1}, and the rightmost dashed vertical line corresponds to $t^*_{c_1} = -t_{c_1} \ln t_{c_1}/t_{s_1}$. The lower dotted horizontal line corresponds to the scaled characteristic value ℓs_2^λ. The constants (without units) used in the numerical simulation are: $e_1^0 = 1$, $s_1^0 = 100$, $e_2^0 = 100$, $k_1 = 0.01$, $k_2 = 1$, $k_3 = 10$, $k_{-3} = 1$, $k_4 = 100$ and $k_{-1} = 1$. Time has been mapped to the t_∞ scale: $t_\infty(t) = 1 - 1/\ln[t + \exp(1)]$, and c_2 has been numerically scaled by its maximum value.

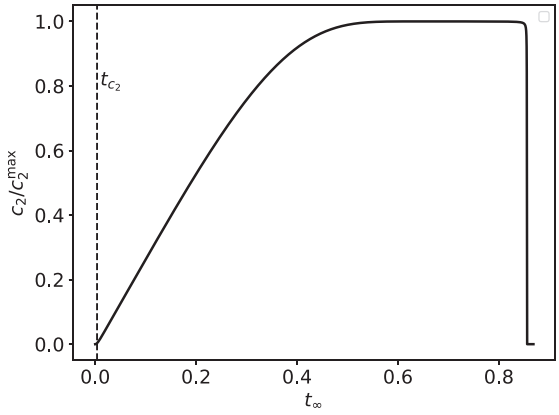

Fig. 12. No significant change in the concentration of s_2 or c_2 occurs over the timescale t_{c_2} in the auxiliary reaction mechanism (47)–(48) when $t_{c_1} \ll t_{c_2} \ll t_{s_2} \ll t_{s_1}$. The thick black curve is the numerically-integrated solutions to the mass action Eqs. (49a)–(49d). The dashed vertical line corresponds to t_{c_2} Note that there is no significant increase in the concentration of the intermediate complex over the t_{c_2} timescale. The constants (without units) used in the numerical simulation are: $e_1^0 = 1$, $s_1^0 = 1000$, $e_2^0 = 1$, $k_1 = 1$, $k_2 = 1$, $k_3 = 1$, $k_{-3} = 1$, $k_4 = 100$ and $k_{-1} = 1$. Time has been mapped to the t_∞ scale: $t_\infty(t) = 1 - 1/\ln[t + \exp(1)]$, and c_2 has been scaled its maximum value.

$$\varpi \frac{d\hat{c}_1}{d\bar{\tau}} = \left[\hat{s}_1 - (1-\beta_1)\hat{c}_1\hat{s}_1 - \beta_1\hat{c}_1\right], \tag{96b}$$

$$\frac{d\hat{s}_2}{d\bar{\tau}} = \nu^{-1}\left[-\hat{s}_2 + (1-\beta_2)\hat{c}_2\hat{s}_2 + \beta_2\alpha_2\hat{c}_2\right] + r_S\mu_2\hat{c}_1, \tag{96c}$$

$$\frac{d\hat{c}_2}{d\bar{\tau}} = (1+\kappa_2)(1+\sigma_2)\left[\hat{s}_2 - (1-\beta_2)\hat{c}_2\hat{s}_2 - \beta_2\hat{c}_2\right]. \tag{96d}$$

If $\nu^{-1} \ll 1$, then we immediately see that

$$\frac{d\hat{s}_2}{d\bar{\tau}} \simeq r_S\mu_2\hat{c}_1 + \mathcal{O}(\nu^{-1}). \tag{97}$$

Next, because we have assumed in our ordering that $t_{c_1} \ll t_{c_2}$, Eq. (97) can be reduced further by noting that $\hat{c}_1 \simeq 1$:

$$\frac{d\hat{s}_2}{d\bar{\tau}} \simeq r_S\mu_2. \tag{98}$$

If we can then find a bound on $r_S\mu_2$ by showing that $r_S\mu_2 \leq K$ and $K \sim \nu^{-1}$, then it follows that s_2 is a *slow* variable with respect to $\bar{\tau}$. Expanding $r_S\lambda_2$ yields

$$r_S\mu_2 = \frac{s_1^0}{s_2^{\max}}\frac{t_{c_2}}{t_{s_1}} = \frac{e_2^0}{K_{M_2}} - \varepsilon_1\frac{k_2 s_1^0}{K_{M_2}k_4} \geq 0, \tag{99}$$

which implies

$$r_S\mu_2 \leq \frac{e_2^0}{K_{M_2}} \equiv K \leq \nu^{-1}. \tag{100}$$

Thus, based on the scaling analysis, we take $s_2 \simeq 0$ for $t \leq t_{c_2}$. The immediate consequence is that $c_2 \simeq 0$ for $t \leq t_{c_2}$, since complex cannot form without the presence of substrate. Thus, no significant change in the concentration of s_2 or c_2 occurs for $t \leq t_{c_2}$ when $t_{c_1} \ll t_{c_2} \ll t_{s_2} \ll t_{s_1}$ (see Fig. 12).

Next, we scale with respect to the slow timescale, $\bar{T}$:

$$\frac{d\hat{s}_1}{d\bar{T}} = \mu_1(1+\kappa_1)(1+\sigma_1)\left[-\hat{s}_1 + (1-\beta_1)\hat{c}_1\hat{s}_1 + \beta_1\alpha_1\hat{c}_1\right], \tag{101a}$$

$$\varepsilon_1\frac{d\hat{c}_1}{d\bar{T}} = \mu_1(1+\kappa_1)(1+\sigma_1)\left[\hat{s}_1 - (1-\beta_1)\hat{c}_1\hat{s}_1 - \beta_1\hat{c}_1\right] \tag{101b}$$

$$\frac{d\hat{s}_2}{d\bar{T}} = -\hat{s}_2 + (1-\beta_2)\hat{c}_2\hat{s}_2 + \beta_2\alpha_2\hat{c}_2 + r_S\mu_1\hat{c}_1, \tag{101c}$$

$$\epsilon\frac{d\hat{c}_2}{d\bar{T}} = \hat{s}_2 - (1-\beta_2)\hat{c}_2\hat{s}_2 - \beta_2\hat{c}_2. \tag{101d}$$

The term $r_S\mu_1$ is $\mathcal{O}(1)$, and $\hat{c}_2$ can be approximated as being in QSS since $\epsilon \ll 1$ when $t_{c_2} \ll t_{s_2}$. Putting these observations together yields the dimensional equation

$$\dot{s}_2 \simeq -\frac{V_2}{K_{M_2} + s_2}s_2 + k_2c_1^{\max}, \quad t \lesssim t_{s_2}, \tag{102}$$

which admits an exact solution in the form of a Lambert-W function

$$s_2 \simeq s_2^{\max}(1 + \psi W\left[-\psi^{-1}\exp(-\psi^{-1} - \Theta\cdot t)\right]), \quad t \lesssim t_{s_2}, \tag{103}$$

where $\psi \equiv V_2/(k_2c_1^{\max})$ and $\Theta \equiv (V_2 - k_2c_1^{\max})^2/(V_2K_{M_2})$. From (103), we have a new timescale, $t^\chi_{s_2}$:

$$t^\chi_{s_2} \equiv \frac{K_{M_2} + s_2^{\max}}{V_2}. \tag{104}$$

Since no significant change in the concentration of any chemical species occurs over t_{c_2}, the *kinetic* analysis in this regime can be effectively carried out with *three* timescales: $t_{c_1}, t^\chi_{s_2}, t_{s_1}$ (Eilertsen and Schnell, 2018). Additionally, it is also worth noting that rescaling the mass action equations with respect to $T^\chi = t/t^\chi_{s_2}$ yields,

$$\frac{d\hat{s}_1}{dT^\chi} = \frac{t^\chi_{s_2}}{t_{s_1}}(1+\kappa_1)(1+\sigma_1)\left[-\hat{s}_1 + (1-\beta_1)\hat{c}_1\hat{s}_1 + \beta_1\alpha_1\hat{c}_1\right], \tag{105a}$$

$$\frac{t_{c_1}}{t^\chi_{s_2}}\frac{d\hat{c}_1}{dT^\chi} = \hat{s}_1 - (1-\beta_1)\hat{c}_1\hat{s}_1 - \beta_1\hat{c}_1, \tag{105b}$$

$$\frac{d\hat{s}_2}{dT^\chi} = (1+\kappa_2)(1+\sigma_2)\left[-\hat{s}_2 + (1-\beta_2)\hat{c}_2\hat{s}_2 + \beta_2\alpha_2\hat{c}_2\right] + \hat{c}_1, \tag{105c}$$

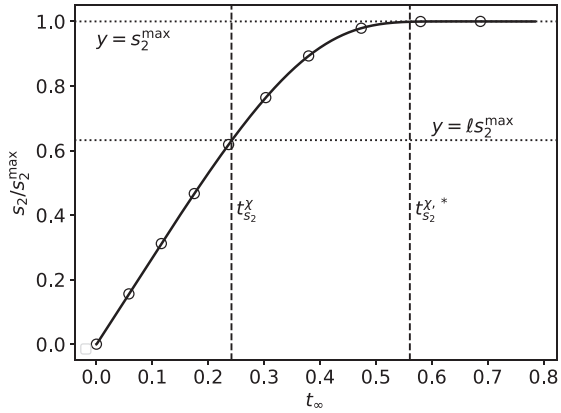

Fig. 13. The validity of $t_{s_2}^{\chi}$ and $t_{s_2}^{\chi,*}$ in the auxiliary reaction mechanism (47)–(48) when $\epsilon \ll 1$. The thick black curve is the numerically-integrated solution to the mass action Eq. (49a)–(49d), and the unfilled circles mark the inner solution given by (103). The leftmost dashed vertical line corresponds to $t_{s_2}^{\chi}$, and the rightmost dashed vertical line corresponds to $t_{s_2}^{\chi,*} = -t_{s_2}^{\chi} \ln t_{s_2}^{\chi}/t_{s_1}$. The lower dotted horizontal line corresponds to $y = \ell s_2^{\max}$, and the upper dotted horizontal line corresponds to $y = s_2^{\max}$. The constants (without units) used in the numerical simulation are: $e_1^0 = 1$, $s_1^0 = 1000$, $e_2^0 = 1$, $k_1 = 1$, $k_2 = 1$, $k_3 = 1$, $k_{-3} = 1$, $k_4 = 100$ and $k_{-1} = 1$. Time has been mapped to the t_∞ scale: $t_\infty(t) = 1 - 1/\ln[t + \exp(1)]$, and s_2 has been numerically scaled by its maximum value. Note that the mass action equations have only been integrated from $t = 0$ to $t \approx t_{s_2}^{\chi,*}$ for clarity.

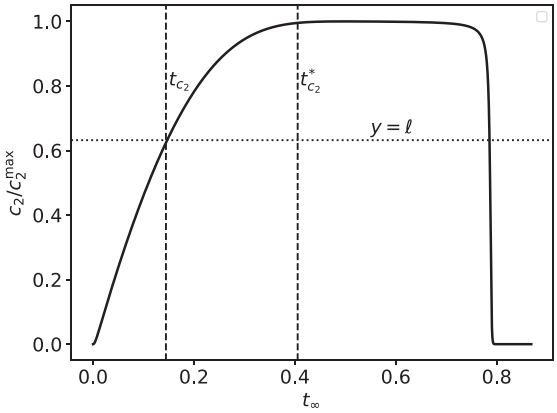

Fig. 14. The lag time in the auxiliary reaction mechanism (47)–(48) when $t_{s_2} \ll t_{c_1} \ll t_{c_2} \ll t_{s_1}$. The thick black curve is the numerically-integrated solution to the mass action Eqs. (49a)–(49d), and the unfilled circles mark the inner solution given by (103). The leftmost dashed vertical line corresponds to t_{c_2}, and the rightmost dashed vertical line corresponds to $t_{c_2}^* = -t_{c_2} \ln t_{c_2}/t_{s_1}$. The lower dotted horizontal line corresponds to $y = \ell$; The constants (without units) used in the numerical simulation are: $e_1^0 = 1$, $s_1^0 = 1000$, $e_2^0 = 1$, $k_1 = 1$, $k_2 = 1$, $k_3 = 1$, $k_{-3} = 1$, $k_4 = 100$ and $k_{-1} = 1$. Time has been mapped to the t_∞ scale: $t_\infty(t) = 1 - 1/\ln[t + \exp(1)]$, and c_2 has been numericallyscaled by its maximum value.

$$\epsilon \frac{d\hat{c}_2}{dT^{\chi}} = (1+\kappa_2)(1+\sigma_2)\big[\hat{s}_2 - (1-\beta_2)\hat{c}_2\hat{s}_2 - \beta_2\hat{c}_2\big], \tag{105d}$$

and the term in front of $\hat{c}_1$ in (105c) is equal to 1. It follows that (105c) is, to leading order, given by

$$\frac{d\hat{s}_2}{dT^{\chi}} \simeq -\frac{\hat{s}_2(1+\sigma_2)}{1+\sigma_2\hat{s}_2} + 1. \tag{106}$$

Furthermore, rescaling the mass action equations with respect to T yields

$$\frac{d\hat{s}_1}{dT} = (1+\kappa_1)(1+\sigma_1)\big[-\hat{s}_1 + (1-\beta_1)\hat{c}_1\hat{s}_1 + \beta_1\alpha_1\hat{c}_1\big], \tag{107a}$$

$$\varepsilon_2 \frac{d\hat{c}_1}{dT} = \hat{s}_1 - (1-\beta_1)\hat{c}_1\hat{s}_1 - \beta_1\hat{c}_1, \tag{107b}$$

$$\frac{t_{s_2}^{\chi}}{t_{s_1}}\frac{d\hat{s}_2}{dT} = (1+\kappa_2)(1+\sigma_2)\big[-\hat{s}_2 + (1-\beta_2)\hat{c}_2\hat{s}_2 + \beta_2\alpha_2\hat{c}_2\big] + \hat{c}_1, \tag{107c}$$

$$\mu_2 \frac{d\hat{c}_2}{dT} = (1+\kappa_2)(1+\sigma_2)\big[\hat{s}_2 - (1-\beta_2)\hat{c}_2\hat{s}_2 - \beta_2\hat{c}_2\big], \tag{107d}$$

from which it directly follows (see Fig. 13) that the time it takes for $\dot{p}$ to reach its maximum is given by

$$t_{s_2}^{\chi,*} \approx -t_{s_2}^{\chi} \ln \frac{t_{s_2}^{\chi}}{t_{s_1}}. \tag{108}$$

The timescale (108) is the matching timescale for s_2. It is a very good estimate of the time it takes s_2 to reach QSS, and corresponds to the time it takes the phase-plane trajectory to reach $\boldsymbol{x}^*$ when $\epsilon \ll 1$ (Eilertsen and Schnell, 2018).

5.2. Scaling analysis: $t_{c_2} \ll t_{c_1} \ll t_{s_2} \ll t_{s_1}$

In the previous subsection we showed that t_{c_2} was a "hidden" timescale: no significant accumulation of s_2 and c_2 occurs over t_{c_2} when $t_{c_1} \ll t_{c_2} \ll t_{s_2} \ll t_{s_1}$. In this subsection we examine was what happens when $t_{c_2} \ll t_{c_1}$. First, note that

$$\lim_{k_4 \to \infty} t_{s_2}^{\chi} = t_{s_2}, \tag{109}$$

and second,

$$\lim_{k_4 \to \infty} c_2^{\max} = 0, \quad \text{and} \quad \lim_{k_4 \to \infty} s_2^{\max} = s_2^{\lambda}. \tag{110}$$

Finally, since

$$W\big[-\psi^{-1}\exp(-\psi^{-1} - \Theta \cdot t)\big] \simeq -\psi^{-1}\exp(-\psi^{-1} - \Theta \cdot t), \quad \psi^{-1} \ll 1, \tag{111}$$

we can combine (109), (110) and (111) to yield

$$s_2 \approx s_2^{\lambda}[1 - \exp(-t/t_{s_2})], \quad \text{for } t \lesssim t_{s_2}. \tag{112}$$

From a geometrical point of view, the c_2-nullcline gets pressed against the s_2-axis in the phase-plane as $k_4 \to \infty$, and $c_2^{\max}$ is almost negligible in magnitude. Thus, when $k_4 \gg k_3 e_2^0$, the mass action kinetics can *essentially* be approximated by (112), since $t_{s_2} \approx t_{s_2}^{\chi}$ and $s_2^{\max} \approx s_2^{\lambda}$ as $t_{c_2} \to 0$. Consequently, t_{s_2} is approximately characteristic of the time it takes s_2 to reach $s_2^{\max}$ in regimes where t_{c_2} is a *super-fast* timescale and $t_{c_2} \ll t_{c_1} \ll t_{s_2}^{\chi} \ll t_{s_1}$.

5.3. Scaling analysis: $t_{s_2} \ll t_{c_1} \ll t_{c_2} \ll t_{s_1}$

Another case is when t_{s_2} is a super-fast timescale. Under this scenerio, the scaled equations indicate that s_2 is in QSS for the duration of the reaction. Geometrically, s_2 will closely follow the s_2-nullcline as it moves in the s_2–c_2 phase–plane. In this case c_2 is asymptotic to

$$\dot{c}_2 \simeq -k_4 c_2 + k_2 c_1, \quad t \geq 0, \tag{113}$$

and thus t_{c_2} remains characteristic of the time is takes c_2 to reach its maximum value, and the matching timescale $t_{c_2}^*$ provides an estimate for the time it takes for $\dot{p}$ to reach its maximum value (see Fig. 14).

5.4. Scaling analysis: $t_{c_1} \ll t_{c_2} \approx t_{s_2} \ll t_{s_1}$

Up until this point, we have been able to derive characteristic timescales that quantify the temporal order of magnitude of a specific trajectory's rapid approach to QSS. Our success in the derivation of characteristic timescales resides in the fact that, so far, we

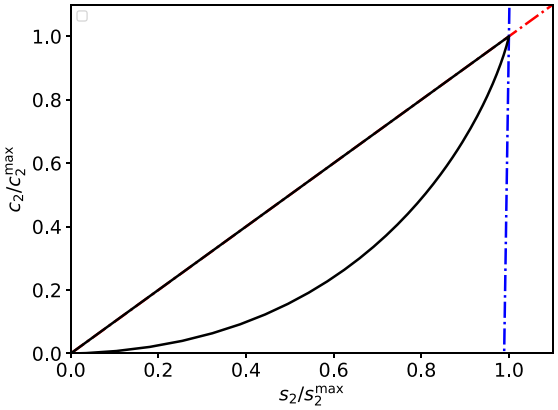

Fig. 15. Phase–plane dynamics of the auxiliary reaction mechanism (47)–(48) when $t_{c_1} \ll t_{c_2} \approx t_{s_2} \ll t_{s_1}$. The thick black curve is the numerically-integrated solution to the mass action Eqs. (49a)–(49d), the dashed/dotted red curve is the c_2-nullcline and the dashed/dotted blue curve is the stationary s_2-nullcline. Notice that the trajectory does not follow a path that lies close to either nullcline in the approach to $\boldsymbol{x}^*$. The constants (without units) used in the numerical simulation are: $e_1^0 = 1,\ s_1^0 = 1000,\ e_2^0 = 10,\ k_1 = 1,\ k_2 = 1,\ k_3 = 10,\ k_{-3} = 1,\ k_4 = 100$ and $k_{-1} = 1$. (For interpretation of the references to colour in this figure legend, the reader is referred to the web version of this article.)

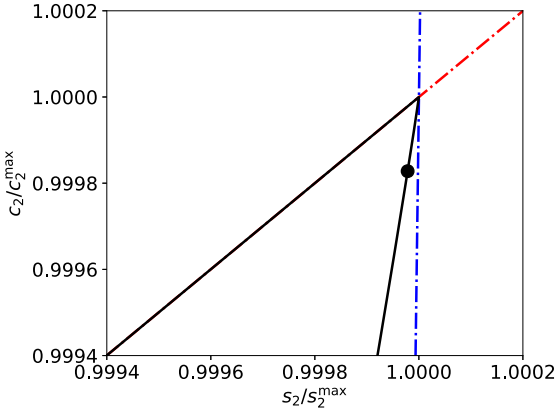

Fig. 16. The lag time in the auxiliary reaction mechanism (47)–(48) when $t_{c_1} \ll t_{c_2} = t_{s_2} \ll t_{s_1}$. This is a close-up of Fig. 15 near $\boldsymbol{x}^*$. The thick black curve is the numerically-integrated solution to the mass action Eqs. (49a)–(49d), the dashed/dotted red curve is the c_2-nullcline and the dashed/dotted blue curve is the stationary s_2-nullcline. The solid black circle marks the trajectory when $t = t_{s_2}^* = -t_{s_2} \ln t_{s_2}/t_{s_1}$. Notice that Tikhonov's Theorem still provides a reasonable estimate of the lag time, which is synonymous with the matching timescale corresponding to either s_2 or c_2. The constants (without units) used in the numerical simulation are: $e_1^0 = 1,\ s_1^0 = 1000,\ e_2^0 = 10,\ k_1 = 1,\ k_2 = 1,\ k_3 = 10,\ k_{-3} = 1,\ k_4 = 100$ and $k_{-1} = 1$. (For interpretation of the references to colour in this figure legend, the reader is referred to the web version of this article.)

have only considered regimes in which trajectories are asymptotic manifolds (i.e., the s_2-nullcline or the c_2-nullcline) in their approach to $\boldsymbol{x}^*$. However, their are many such trajectories that are not asymptotic to a particular manifold in the approach to $\boldsymbol{x}^*$. For example, if $t_{c_1} \ll t_{c_2} \approx t_{s_2} \ll t_{s_1}$, then it is obvious from both the scaling analysis and the phase-plane dynamics that the trajectory will not follow closely to either nullcline in its approach to $\boldsymbol{x}^*$ (see Fig. 15). It is not obvious in this case how to go about determining the lag time. However, Theorem 1 suggests that either matching timescale $t_{c_2}^*$ or $t_{s_2}^*$ should yield a reasonable approximation to the lag time. Thus, even though the transient solution is unknown, the scaling analysis still provides a good estimate of the time it takes for the secondary reaction to "catch" the primary reaction and for $\dot{p}$ to reach its maximum value (see Fig. 16).

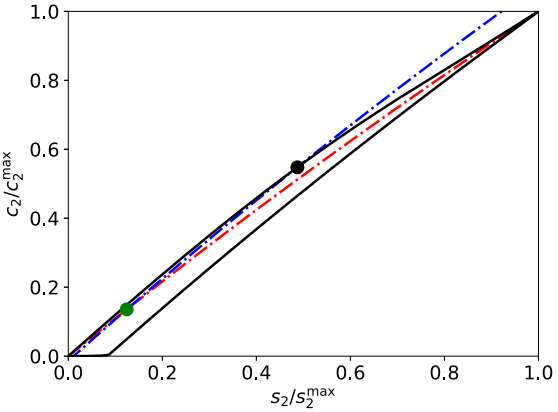

Fig. 17. The trajectory follows the s_2-nullcline in the phase–plane of the auxiliary reaction mechanism (47)–(48) when $t_{s_2}^{\chi}/t_{s_1} \ll 1$. The thick black curve is the numerically-integrated solution to the mass action Eqs. (49a)–(49d), the dashed/dotted red curve is the c_2-nullcline and the dashed/dotted blue curve is a snapshot of s_2-nullcline when $t \approx 1.1 \cdot t_{s_1}$. The green dot is the intersection of the nullclines; the black dot is the corresponding snapshot of the numerical solution to (49a)–(49d). In this simulation, $t_{s_2}^{\chi}/t_{s_1} \approx 0.001 < \mu_2 \approx 0.1$; consequently, the trajectory follows the s_2-nullcline but fails to closely follow $\boldsymbol{x}^*$ (see Movie 1 in Supplementary Materials). The constants (without units) used in the numerical simulation are: $e_1^0 = 1,\ s_1^0 = 100,\ e_2^0 = 100,\ k_1 = 1,\ k_2 = 1,\ k_3 = 1,\ k_{-3} = 1,\ k_4 = 0.1$ and $k_{-1} = 1$. (For interpretation of the references to colour in this figure legend, the reader is referred to the web version of this article.)

6. The region of validity of the timescale estimations

We conclude our analysis by noting that the conditions $\max\{\varepsilon_2, \mu_1, \mu_2\} \ll 1$ do not provide a *universal* set of qualifiers to ensure that the phase-plane trajectory approximately adheres to $\boldsymbol{x}^*$ after a brief fast transient. To establish criteria that determines a region in parameter space within which our analysis is valid, we first remark that an absolutely necessary condition for the validity of our timescale analysis is $V_2 \gg k_2 c_1^{\max}$. Second, if $V_2 \gg k_2 c_1^{\max}$ holds, then $0 < t_{s_2} < t_{s_2}^{\chi}$ since

$$t_{s_2}^{\chi} = t_{s_2}(1+\kappa_2)\big[1 + \theta + \mathcal{O}(\theta^2)\big], \quad \theta \equiv \frac{k_2 c_1^{\max}}{V_2}. \tag{114}$$

Consequently, we take

$$0 < \min\{t_{s_2}^{\chi}/t_{s_1}, t_{c_2}/t_{s_1}\}, \tag{115a}$$

$$\max\{t_{s_2}^{\chi}/t_{s_1}, t_{c_2}/t_{s_1}\} \ll 1, \tag{115b}$$

as our qualifying set of conditions that must hold in order for the trajectory to closely follow $\boldsymbol{x}^*$. This implies that the natural scaling to employ is given by (107c)–(107d), and gives a universal set of parameters from which to analyze the phase-plane dynamics. For example, if $t_{s_2}^{\chi} \ll t_{s_1}$ but $\mu_2 \sim 1$, then we do not expect the trajectory to closely follow $\boldsymbol{x}^*$. However, we see from the scaled equations that s_2 should deplete in a QSS over the t_{s_1} timescale as long as $t_{s_2}^{\chi} \ll t_{s_1}$. Thus, the trajectory s_2 "sticks" to the s_2-nullcline, but lags behind $\boldsymbol{x}^*$ since $\mu_2 \sim 1$ (see Fig. 17). On the other hand, when the phase-plane trajectory does closely follow $\boldsymbol{x}^*$, the scaling given by (107c)–(107d) tells us the component that contributes most to the error in our approximation (see Fig. 18).

7. Discussion

Enzyme catalyzed reactions typically exhibit multiple dynamical regimes; each regime marks a domain over which certain kinetic behavior and approximate rate laws can be assumed to be valid. The approximate rate laws are derived assuming timescale

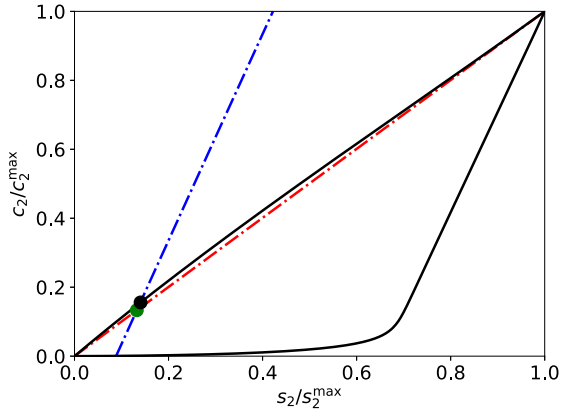

Fig. 18. The component-wise error when the indicator reaction is fast in the auxiliary reaction mechanism (47)–(48). The thick black curve is the numerically-integrated solution to the mass action Eqs. (49a)–(49d), the dashed/dotted red curve is the c_2-nullcline and the dashed/dotted blue curve is a snapshot of s_2-nullcline when $t \approx 1.1 \cdot t_{s_1}$. The black dot is the corresponding snapshot of the numerical solution to (49a)–(49d). In this simulation, $t_{s_2}^{\chi}/t_{s_1} \approx 0.0001 < \mu_2 \approx 0.005$; consequently, the trajectory sits "just behind" and slightly above $\boldsymbol{x}^*$ (green dot) since the trajectory will be closer to the s_2-nullcline than the c_2-nullcline (see Movie 2 in Supplementary Materials). The constants (without units) used in the numerical simulation are: $e_1^0 = 1$, $s_1^0 = 100$, $e_2^0 = 100$, $k_1 = 1$, $k_2 = 1$, $k_3 = 1$, $k_{-3} = 1$, $k_4 = 2$ and $k_{-1} = 1$. (For interpretation of the references to colour in this figure legend, the reader is referred to the web version of this article.)

separations. The primary contribution of this paper is to categorize specific types of timescales, particularly with regard to matched asymptotics in enzyme catalyzed reactions. In short, we have shown that in each kinetic regime of a reaction there really exist two distinct timescales that must be considered: characteristic and matching. Characteristic timescales arise naturally when the initial fast transient of a reaction can be approximated with a linear equation. This happens often in enzyme catalyzed models, since the differential equation governing the fast variable becomes linear when the slow variable is held constant. As such, the characteristic timescale should be utilized in scaling analysis, since it determines the relevant length scale of its corresponding regime. However, its limitation resides in the fact that it does not provide a good approximation to the time it takes a reaction to reach QSS. The matching timescale provides a reliable estimate to reach QSS, and determines the temporal boundary of the corresponding regime.

In this work, the fast and slow timescales of the single-enzyme, single-substrate MM reaction mechanism (12) have been revisited. Under the RSA, the established fast timescale, t_{c_1}, of the MM reaction mechanism is a characteristic timescale: it provides the temporal order of magnitude needed for the concentration of complex to accumulate to approximately 63% of its threshold value. This is *the* appropriate timescale to utilize in the scaling analysis. However, since t_{c_1} does not provide a good estimate of when the complex concentration reaches its maximum value, it fails to define an appropriate matching timescale. The matching timescale delimits the approximate time point in the course of the reaction when the transition from initial fast transient to quasi-steady-state kinetics occurs. By utilizing Tikhonov/Fenichel theory, we have shown that the appropriate matching timescale for the MM reaction mechanism is $t_{c_1}^*$:

$$t_{c_1}^* = -t_{c_1} \ln \frac{t_{c_1}}{t_{s_1}}.$$

In this paper, we consider the auxiliary enzyme reaction mechanism (47)–(48) as a multiple timescale case study. This reaction was initially analyzed with the assumption that the auxiliary enzyme concentration is high, and that the primary reaction obeys the RSA. We demonstrated that when the secondary reaction has sufficient speed, the overall kinetics and reaction mechanism is determined by the ratios of four timescales: t_{c_1}, t_{s_2}, t_{c_2} and t_{s_1}. Six different orderings of these timescales were considered: (i) $t_{c_1} \ll t_{s_2} \ll t_{c_2} \ll t_{s_1}$, (ii) $t_{c_1} \ll t_{c_2} \ll t_{s_2} \ll t_{s_1}$, (iii) $\{t_{c_2}, t_{s_2}\} \ll t_{c_1} \ll t_{s_1}$, (iv) $t_{c_2} \ll t_{c_1} \ll t_{s_2} \ll t_{s_1}$, (v) $t_{s_2} \ll t_{c_1} \ll t_{c_2} \ll t_{s_1}$, and (vi) $t_{c_1} \ll t_{s_2} = t_{c_2} \ll t_{s_1}$. The lag time, which is roughly the time it takes for the rate of product generation to reach its maximum value, was calculated for each specific ordering. As we have shown, the lag time corresponds to a specific matching timescale; specifically, we have demonstrated that the lag time is synonymous with the matching timescale that corresponds to the slow variable when the auxiliary reaction is composed of super-fast, fast, slow and super-slow variables.

The estimation of timescales is perhaps the most challenging component of chemical kinetics. The subtle difference between characteristic and matching timescales is often neglected in applications of GSPT. This work provides a useful case study in the interpretation of timescales in enzyme-catalyzed reactions, and the approaches used should be readily applicable to a wide range of singular perturbation problems in mathematical biology.

On a final note, we wish to emphasize that we carried out this analysis by restricting the parameters pertinent to the primary reaction to lie in a regime in which the RSA and QSSA are applicable. This is of course not necessary, and the total quasi-steady-state approximation (tQSSA) could have been employed (Bersani et al., 2015; Bersani and Dell'Acqua, 2012; Borghans et al., 1996; Schnell and Maini, 2002; Tzafriri, 2003). The tQSSA is lumping method that is generally considered to be valid over a much larger parameter range than the QSSA. It has been applied to complex enzyme catalyzed reactions that exhibit both reversibility (Tzafriri and Edelman, 2004) and competition (Pedersen et al., 2006). From a timescale perspective, the tQSSA has an advantage it reduces the total number of timescales in the system by lumping two chemical species into one by defining the total substrate $s_T = c_1 + s_1$. The disadvantage of this approach is that the lumping of variables inevitably leads to a lower dimensionality system with a potentially different dynamical behavior. So far, the validity and applicability of the tQSSA in the case of both the auxiliary reaction and coupled zymogen activation reactions (Eilertsen et al., 2018) remains open, and we certainly encourage exploration and research in this direction.

Acknowledgements

This work is partially supported by the University of Michigan Protein Folding Diseases Initiative, and Beilstein-Institut zur Förderung der Chemischen Wissenschaften through its Beilstein Enzymology Symposia. We are grateful to Antonio Baici (University of Zurich) for helpful discussions about this work during the 2017 Beilstein Enzymology Symposia (Rüdesheim, Germany. WS is partially funded through the Michigan IRACDA program (NIH/NIGMS grant: K12 GM111725).

Supplementary material

Supplementary material associated with this article can be found, in the online version, at doi:10.1016/j.jtbi.2019.01.005.

References

Berglund, N., Gentz, B., 2006. Noise-Induced Phenomena in Slow-Fast Dynamical Systems. Springer-Verlag London, Ltd., London.

Bersani, A.M., Bersani, E., Dell'Acqua, G., Pedersen, M.G., 2015. New trends and perspectives in nonlinear intracellular dynamics: one century from Michaelis–Menten paper. Contin. Mech. Thermodyn. 27, 659–684.

Bersani, A.M., Dell'Acqua, G., 2012. Is there anything left to say on enzyme kinetic constants and quasi-steady state approximation? J. Math. Chem. 50, 335–344.

Bertram, R., Rubin, J.E., 2017. Multi-timescale systems and fast-slow analysis. Math. Biosci. 287, 105–121.
Borghans, J.A.M., De Boer, R.J., Segel, L.A., 1996. Extending the quasi-steady state approximation by changing variables. Bull. Math. Biol. 58, 43–63.
Burke, M.A., Maini, P.K., Murray, J.D., 1993. Suicide substrate reaction-diffusion equations: varying the source. IMA J. Math. Appl. Med. Biol. 10, 97–114.
Burke, M.A., Maini, P.K., Murray, J.D., 1990. On the kinetics of suicide substrates. Biophys. Chem. 37, 81–90.
Clark, A.R., Stokes, Y.M., Thompson, J.G., 2011. Estimation of glucose uptake by ovarian follicular cells. Ann. Biomed. Eng. 39, 2654–2667.
Corless, R.M., Gonnet, G.H., Hare, D.E.G., Jeffrey, D.J., Knuth, D.E., 1996. On the Lambert *W* function. Adv. Comput. Math. 5, 329–359.
Eilertsen, J., Schnell, S., 2018. A kinetic analysis of coupled (or auxiliary) enzyme reactions. Bull. Math. Biol. 80, 3154–3183.
Eilertsen, J., Stroberg, W., Schnell, S., 2018. A theory of reactant-stationary kinetics for a mechanism of zymogen activation. Biophys. Chem. 242, 34–44.
Espenson, J.H., 1995. Chemical Kinetics and Reaction Mechanisms. McGraw-Hill, Singapore.
Feng, S., Laketa, V., Stein, F., Rutkowska, A., MacNamara, A., Depner, S., Klingmüller, U., Saez-Rodriguez, J., Schultz, C., 2014. A rapidly reversible chemical dimerizer system to study lipid signaling in living cells. Angew. Chem. Int. Ed. 53, 6720–6723.
Fenichel, N., 1971. Persistence and smoothness of invariant manifolds for flows. Indiana Univ. Math. J. 21, 193–226.
Fenichel, N., 1979. Geometric singular perturbation theory for ordinary differential equations. J. Diff. Eqs. 31, 53–98.
Frenzen, C.L., Maini, P.K., 1988. Enzyme kinetics for a two-step enzymic reaction with comparable initial enzyme-substrate ratios. J. Math. Biol. 26, 689–703.
Gallagher, R., 2004. Enzymes make the world go 'round. Scientist 18, 6.
Gradšteĭn, I.S., 1953. Application of A. M. Lyapunov's theory of stability to the theory of differential equations with small coefficients in the derivatives. Mat. Sbornik N. S. 32, 263–286.
Hanson, S.M., Schnell, S., 2008. Reactant stationary approximation in enzyme kinetics. J. Phys. Chem. A 112, 8654–8658.
Heineken, F.G., Tsuchiya, H.M., Aris, R., 1967. On the mathematical status of the pseudo-steady state hypothesis of biochemical kinetics. Math. Biosci. 1, 95–113.
Holmes, M.H., 2013. Introduction to Perturbation Methods, 2nd edition Springer-Verlag, New York.
Klonowski, W., 1983. Simplifying principles for chemical and enzyme reaction kinetics. Biophys. Chem. 18, 73–87.
Kuehn, C., 2015. Multiple time scale dynamics. Springer-Verlag, New York.
Letson, B., Rubin, J.E., Vo, T., 2017. Analysis of interacting local oscillation mechanisms in three-timescale systems. SIAM J. Appl. Math. 77, 1020–1046.
Lin, C.C., Segel, L.A., 1988. Mathematics applied to deterministic problems in the natural sciences, 2nd edition Society for Industrial and Applied Mathematics (SIAM), Philadelphia, PA.
Maini, P.K., Woolley, T.E., Baker, R.E., Gaffney, E.A., Lee, S.S., 2012. Turing's model for biological pattern formation and the robustness problem. Interface Focus 2, 487–496.
Murugan, R., 2018. Theory on the rate equation of Michaelis-Menten type single–substrate enzyme catalyzed reactions. J. Math. Chem. 56, 508–556.
Nan, P., Wang, Y., Kirk, V., Rubin, J.E., 2015. Understanding and distinguishing three--time-scale oscillations: case study in a coupled morris-lecar system. SIAM J. Appl. Dyn. Syst. 14, 1518–1557.
Nguyen, A.H., Fraser, S., 1989. Geometrical picture of reaction in enzyme kinetics. J. Chem. Phys. 91, 186–193.
Palsson, B.O., 1987. On the dynamics of the irreversible Michaelis–Menten reaction mechanism. Chem. Eng. Sci. 42, 447–458.
Palsson, B.O., Lightfoot, E.N., 1984. Mathematical modelling of dynamics and control in metabolic networks. I. On Michaelis-Menten kinetics. J. Theor. Biol. 111, 273–302.
Palsson, B.O., Palsson, H., Lightfoot, E.N., 1985. Mathematical modelling of dynamics and control in metabolic networks. III. Linear reaction sequences. J. Theor. Biol. 113, 231–259.
Pedersen, M.G., Bersani, A.M., Bersani, E., 2007. The total quasi-steady-state approximation for fully competitive enzyme reactions. Bull. Math. Biol. 69, 433–457.
Rice, O.K., 1960. Conditions for a steady state in chemical kinetics. J. Phys. Chem. 64, 1851–1857.
Roussel, M.R., Fraser, S.J., 1990. Geometry of the steady-state approximation: perturbation and accelerated convergence methods. J. Chem. Phys. 93, 1072–1081.
Roussel, M.R., Fraser, S.J., 1991. Accurate steady-state approximations: implications for kinetics experiments and mechanism. J. Phys. Chem. 95, 8762–8770.
Schnell, S., 2014. Validity of the Michaelis-Menten equation – Steady-state, or reactant stationary assumption: that is the question. FEBS J. 281, 464–472.
Schnell, S., Maini, P.K., 2000. Enzyme kinetics at high enzyme concentration. Bull. Math. Biol. 62, 483–499.
Schnell, S., Maini, P.K., 2002. Enzyme kinetics far from the standard quasi-steady-state and equilibrium approximations. Math. Comput. Modelling 35, 137–144.
Schnell, S., Maini, P.K., 2003. A century of enzyme kinetics. Reliability of the K_M and $v_{\max}$ estimates. Comments Theor. Biol. 8, 169–187.
Schnell, S., Mendoza, C., 1997. Closed form solution for time-dependent enzyme kinetics. J. Theor. Biol. 187, 207–212.
Segel, L.A., 1988. On the validity of the steady state assumption of enzyme kinetics. Bull. Math. Biol. 50, 579–593.
Segel, L.A., Slemrod, M., 1989. The quasi-steady-state assumption: a case study in perturbation. SIAM Rev. 31, 446–477.
Shoffner, S.K., Schnell, S., 2017. Approaches for the estimation of timescales in nonlinear dynamical systems: timescale separation in enzyme kinetics as a case study. Math. Biosci. 287, 122–129.
Son, K.J., Shin, D.-S., Kwa, T., You, J., Gao, Y., Revzin, A., 2015. A microsystem integrating photodegradable hydrogel microstructures and reconfigurable microfluidics for single-cell analysis and retrieval. Lab Chip 15, 637–641.
Tikhonov, A., 1952. Systems of differential equations containing small parameters in their derivatives. Mat. Sb. (N.S.) 31, 575–586.
Tzafriri, A., Edelman, E., 2004. The total quasi-steady-state approximation is valid for reversible enzyme kinetics. J. Theor. Biol. 226, 303–313.
Tzafriri, A.R., 2003. Michaelis–Menten kinetics at high enzyme concentrations. Bull. Math. Biol. 65, 1111–1129.
Vo, T., Bertram, R., Wechselberger, M., 2013. Multiple geometric viewpoints of mixed mode dynamics associated with pseudo-plateau bursting. SIAM J. Appl. Dyn. Syst. 12, 789–830.